MODELING OF AMPLITUDE DISTRIBUTION DUE TO IONOSPHERIC SCINTILLATION

VIPARAT TORCHAKUL

A THESIS SUBMITTED IN PARTIAL FULFILLMENT
OF THE REQUIREMENT FOR THE DEGREE OF
MASTER OF ENGINEERING IN TELECOMMUNICATION ENGINEERING
SCHOOL OF GRADUATE STUDIES
KING MONGKUT'S INSTITUTE OF TECHNOLOGY LADKRABANG
2004

ISBN 974-9709-39-X

หัวข้อวิทยานิพนธ์	รูปแบบจำลองของการแจกแจงลักษณะการเปลี่ยนแปลงแอมปลิจูดอย่างกระทันหันเนื่องจากชั้นบรรยากาศไอโอโนสเฟียร์
นักศึกษา	นางสาววิภารัตน์ ตอชะกุล
รหัสนักศึกษา	45061232
ปริญญา	วิศวกรรมศาสตร์มหาบัณฑิต
สาขาวิชา	วิศวกรรมโทรคมนาคม
พ.ศ.	2547
อาจารย์ผู้ควบคุมวิทยานิพนธ์	รศ. นิภา ลีลารุจิ
อาจารย์ผู้ควบคุมวิทยานิพนธ์ร่วม	รศ. ณรงค์ เหมกรณ์

บทคัดย่อ

วิทยานิพนธ์ฉบับนี้นำเสนอแบบจำลองลักษณะทางสถิติของการเปลี่ยนแปลงแอมปลิจูดอย่างกระทันหันเนื่องจากกลุ่มความไม่สม่ำเสมอในชั้นบรรยากาศไอโอโนสเฟียร์ ทั้งในระยะสั้นและในระยะยาว โดยงานวิจัยนี้ได้นำข้อมูลของการเกิดการเปลี่ยนแปลงแอมปลิจูดอย่างกระทันหันในย่านความถี่ C-band, S-band และ ย่านความถี่ VHF มาพิจารณาและศึกษาถึงความรุนแรงของการแกว่งของแอมปลิจูดในย่านความถี่ต่างๆ เพื่อนำมาออกแบบจำลอง ซึ่งย่านความถี่ที่นำมาพิจารณานี้มีความหลากหลายทั้งตำแหน่งที่ตั้ง ช่วงเวลาของข้อมูล และความรุนแรงของการเกิดการเปลี่ยนแปลงแอมปลิจูดอย่างกระทันหัน โดยการออกแบบรูปแบบจำลองในระยะสั้นได้พิจารณาการแจกแจงความหนาแน่นความน่าจะเป็นและการแจกแจงสะสม ซึ่งนำไปเปรียบเทียบกับการแจกแจงแบบเกาส์ และแบบนาคากามิ-m สำหรับการวิเคราะห์ทางสถิติในระยะยาวจะใช้หลักการของการแจกแจงแบบ Moulsley-Vilar มาออกแบบจำลองในระยะยาว รวมทั้งนำไปเปรียบเทียบกับการแจกแจงแบบเกาส์ และการประมาณเชิงวิเคราะห์ เพื่อนำมาเปรียบเทียบกับแบบจำลองใหม่ในระยะยาว ซึ่งแบบจำลองในระยะยาวที่พิจารณาได้นั้นสามารถนำไปใช้ในการประมาณหาค่าเฉลี่ยความน่าจะเป็นอัตราผิดพลาดของการสื่อสารเนื่องจากการเปลี่ยนแปลงแอมปลิจูดอย่างกระทันกรณีมอดูเลตแบบ CPSK และ NCFSK

Thesis Title	Modeling of Amplitude Distribution Due to Ionospheric Scintillation
Student	Miss Viparat Torchakul
Student ID	45061232
Degree	Master of Engineering
Programme	Telecommunication Engineering
Year	2004
Thesis Advisor	Assoc. Prof. Nipha Leelaruji
Thesis Co-advisor	Assoc. Prof. Narong Hemmakorn

ABSTRACT

This thesis presents the statistical model of amplitude scintillation effected by ionospheric irregularities in short-term and long-term. The data of amplitude scintillation on C-band, S-band and VHF are considered to designing the model. These frequencies have various factors such as location, period of data and intensity of amplitude scintillation. The design of new model in short-term is considered to probability density function (pdf) and cumulative distribution function (cdf) for comparison with the Gaussian distribution and the Nakagami-m distribution. The statistical analysis of new model is base on Moulsley-Vilar distribution for design model in long-term and compared with the Gaussian distribution, the Moulsley-Vilar distribution and Analytical approximation. Moreover, the probability density function in long-term can be used for determining the impacts of scintillation effects on communication by theoretical estimation of the average probability of bit error rate for both CPSK and NCFSK modulation.

ACKNOWLEDGEMENTS

Many people played important roles in the development of this thesis, and I was deeply grateful to them. Two people at KMITL were particularly helpful. The first, advisor Assoc. Prof. Nipha Leelaruji and co-advisor Assoc. Prof. Narong Hemmakorn, provided constant support, encouragement, and resources to get the job done.

The many researchers of various lectures and discussion including suggestions provided important insights that helped me to improve the final thesis. They deserved special thanks Prof. Dr. Yoshiaki Moriya of Tokai University, Dr. Takashi Maruyama, Mr. Masabumi Kawamura and Dr. Hisamitsu Minakoshi of Communication Research Laboratory.

Moreover, the thesis could not be done without the indispensable contributions of Miss Khajitpan Makaratat, Mr. Adit Decharat and Mr. Sompong Sukkaewthanom to collect the scintillation data in year 2000-2002. I would like to say thank you for their useful experiment.

Finally, the author was really appreciated to all colleagues for discuss and all kindly, T' Anuchit Waisontia, Mr. Thikumporn Boonchunk, Miss Pattama Poomchosark, Mr. Varasin Yarana and Miss Pattariya Theerapatpaiboon; especially Mr. Kitichai Visessiri, their assistance provided. Above all, I was very grateful to my parents and sister who understand and support me for everything.

Viparat Torchakul

TABLE OF CONTENTS

TABLE OF CONTENTS (to)

LIST OF TABLES

LIST OF FIGURES

Figure Page

LIST OF FIGURES (to)

CHAPTER 1
INTRODUCTION

1.1 Literature of Ionospheric Scintillation Modeling

The propagation of radio waves is mainly related to a random medium, which is necessary to be analyzed propagation phenomena by means of statistical methods. For the most of cases, it is certainly possible to describe the variations in time space of propagation parameters by understanding the statistical distribution because it is very important to the fundamental properties of the probability distributions most commonly used in statistical propagation studies. Recently, the radio engineering requirements have become more stringent and necessary not only more details of information on median signal intensity, but also much more knowledge on fading statistics in ionospheric and tropospheric modes of propagation.

Many papers have shown that information on the mean values of the signal received is not sufficient to characterize the performance of radio communication systems. The variation in time, space and frequency have to be considered as well. For description of communication system performance, it is often to observe the time series of signal fluctuation and characterize these fluctuations as a stochastic process. Furthermore modeling amplitude scintillation is the part of signal fluctuation for the purpose of predicting radio system performance.

In the passage of satellite signals through the ionosphere, fluctuations in amplitude and phase are imposed on the signals due to irregularities or inhomogeneities of the electron density in the F-region and Sporadic-E. These fluctuations are called scintillation. A radio signal traversing through the ionosphere will be modified by irregularities with sizes from a few meters to a few kilometers. Scintillations are variations of amplitude, phase and polarization including angle of arrival. Scintillations can be severe and present problems to the radio operator. Effects of ionospheric scintillation have been observed on frequencies ranging from 30MHz to about 10GHz. Therefore, it is essential to analyzed signal statistics at every frequency. Moreover,

scintillations are particularly severe in tropical regions during evenings around the equinoxes and in the auroral zones [1].

1.2 The Significant of the Study

The ionosphere causes significant propagation effects at frequencies up to at least 10 GHz. The effects may be particularly significant for non-geostationary satellite orbit services below 3 GHz. The experimental data has been presented and/or modeling methods have been developed to use for the prediction of the ionospheric propagation parameters needed in planning satellite systems. The ionospheric effects may influence the design and performance of Integrated Services Digital Network (ISDN) and other radio systems. These data and methods have been found that they are applicable within the natural variability of propagation phenomena for applications in satellite system planning. [2]

In order to assess the problem of degradation caused by scintillation and to work out remedies for a user, two types of information are essential, namely the signal statistics and the scintillation morphology. Although the morphological study provides a global view of the scintillation phenomena, however it must be still augmented by a study of signal statistics, as provided for this thesis.

The thesis is analyzing the statistic of scintillation modeling in ionospheric scintillation. The statistic analysis of amplitude scintillation is designed the new model for short-term and long-term. The short-term is considered to the probability density function and cumulative density function of amplitude scintillation. In addition, the long-term can be evaluated the experiment results of new model to be used in the theoretical of bit error rate.

1.3 The Objective and Chapters' Synopsis of the Thesis

The objective of thesis is designing the model of amplitude distribution for short-term and long-term in VHF, S-band and C-band effected by ionospheric scintillation. It can use both weak and strong scintillation. The short-term amplitude scintillation are analyzed the probability density function and cumulative density function by Gaussian distribution, Nakagami-m distribution and new model. While Long-term analysis are

calculated by Moulsley-Vilar model and analytical approximation. Based on application of Moulsley-Vilar model, the experiment results of new model are applied in long-term. Moreover, model in Long-term can be estimated the average probability of bit error rate for some digital modulation condition.

The method and results are provided in this thesis as follows:

Chapter 2 discusses the theoretical background of ionospheric scintillation and factor of amplitude scintillation and describes the scintillation intensity by S_4 index.

Chapter 3 indicates the experiment system and describes the analysis process of each frequency; moreover, presents the analysis of statistical amplitude distribution by probability density function, cumulative distribution function of experiment distribution compared with Gaussian, Nakagami-m distribution and the new model in short-term amplitude scintillation.

Chapter 4 presents the model of amplitude scintillation in long-term and comparison with Moulsley-Vilar distribution, analytical approximation including experimental results of the new model in long-term. In addition, the average probabilities of bit error rate are estimated by experimental results of the new model, which presents the communication impacts for NCFSK and CPSK modulation scheme.

Chapter 5 summarizes the experiment results in short-term and long-term amplitude scintillation distribution.

Finally, Appendix A presents the analysis of new model by Non-linear regression and Bayes' Theorem. Furthermore Appendix B describes the correlation coefficient.

CHAPTER 2

IONOSPHERIC AMPLITUDE SCINTILLATION

One of the most severe disruptions along the transionospheric propagation path for signals below 3 GHz is caused by ionospheric scintillation. Principally through the mechanisms of forward scattering and diffraction, small-scale irregular structures in the ionization density cause scintillation phenomena in which one replaces the steady signal at the receiver. That is fluctuating in amplitude, phase and apparent direction of arrival. Ionospheric scintillation causes both enhancements and fading about the median level as the radio signal transits through the disturbed ionospheric region. Amplitude scintillations can be characterized by a depth of fading and a fading period or frequency. Scintillation effects are the most severe at high latitudes (within and poleward of the auroral region) and in the equatorial region in the post-sunset to midnight local-time sector. Effects on systems range from loss of signal in deep fades cause loss of information or even loss of lock on the signal.

2.1 Ionospheric Scintillation

Ionospheric scintillation, which manifests itself as increased noise on a radio signal intensity and phase, is caused by small-scale variations in the ionospheric electron density along the transionospheric propagation path between the transmitter and receiver. In the Figure 2.1 indicates the result of ionospheric scintillation occur when the irregularities in F and E_s layer pass through the satellite-earth path. These irregularities in the ionosphere introduce fading and enhancement of amplitude, fluctuation, and angle of arrival variation, all the previous effects are ionospheric scintillation. The F region is subdivided into the F_1 layer and the F_2 layer, which are produced by solar extreme ultraviolet light (EUV). At night, scintillations are predominantly an F-Layer phenomenon with irregularities covering the height range from 200 km to 600 km. Below the F region is the E region, which contains both the normal E layer and patches of sporadic E layer (E_s) produced by solar sort X-rays. Sporadic E occurs in range of height from about 90 km to 140 km, as shown in Figure 2.2. In the daytime scintillation is

produced by sporadic E [3]. From the global point of view, there are three major sectors of scintillation activity. The outline of the geomagnetic latitudinal ranges that shall pertain to the labels of high, low and mid-latitudes.

- high-latitudes: $60^{\circ} - 90^{\circ}$
- mid-latitudes: $20^{\circ} - 60^{\circ}$
- low-latitudes: $0^{\circ} - 20^{\circ}$

Even though these ranges are not arbitrarily defined, they are selected as the regions in which specific ionospheric processes take place. The low latitude region is the sector in which equatorial ionospheric effects are the most important, such as the equatorial electrojet, while the high latitude region covers those areas in which polar and auroral ionospheric effects are noteworthy high-energy particle precipitation. The pictures of global scintillation in Figure 2.3 and 2.5 show the important of equatorial and auroral/polar, regions. The equatorial scintillations are, on the whole, stronger than those in high latitudes. Scintillation occurs in middle latitudes but they are less intense than elsewhere and do not present a serious problem.

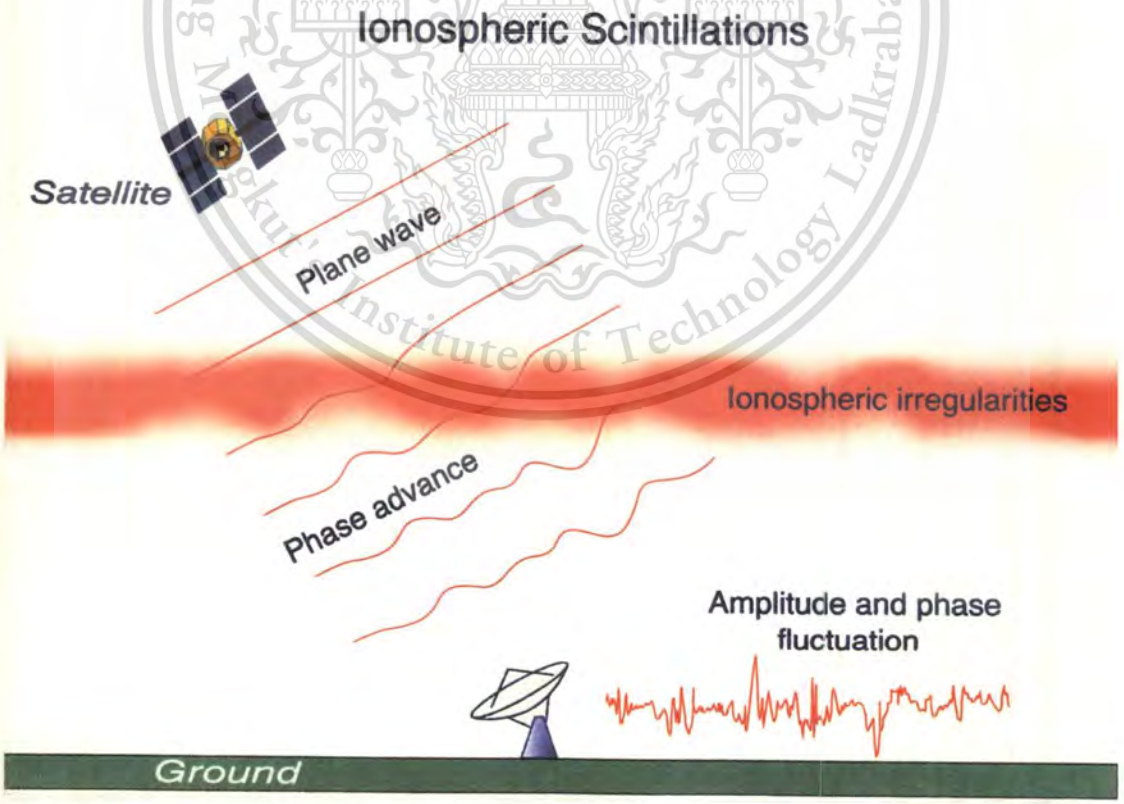

Figure 2.1 Ionospheric scintillation occurs when the irregularities in F and E_s layer pass through in the satellite-earth path [5].

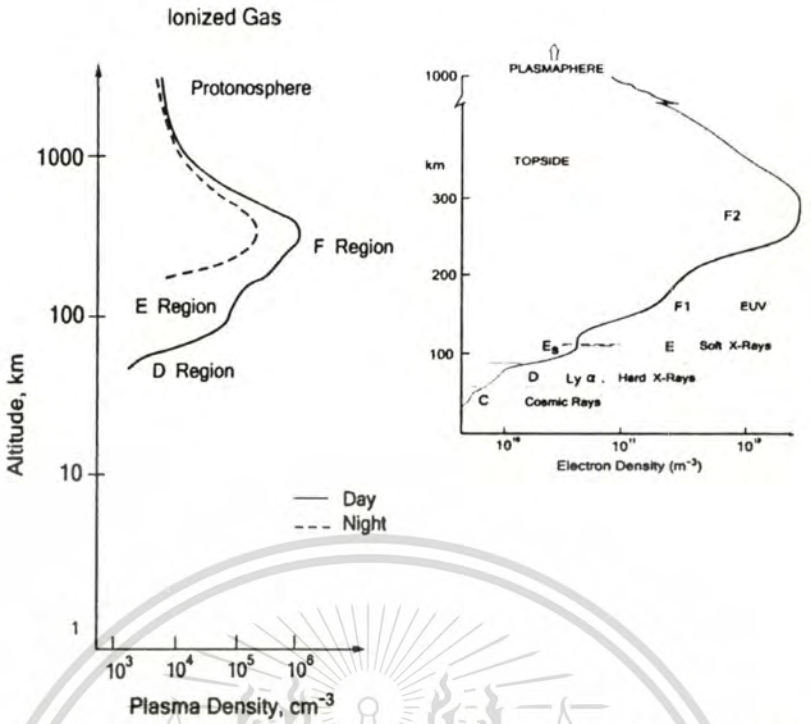

Figure 2.2 Typical profiles of ionospheric plasma density with the various layers designated [3].

2.2 Ionospheric Scintillation Characteristic

The important feature of ionospheric scintillation characteristic and correlation can be summarized as follows:

2.2.1 Diurnal and Seasonal variations

All sectors in Figure 2.3 and 2.5, there is a pronounced nighttime maximum. At equator, the activity only appears after sunset. Even in the polar region, these appear to be greater scintillation occurrence during dark months than during the months of continuous solar visibility. For equatorial gigahertz scintillation, peak activity around the vernal equinox and high activity at the autumnal equinox have been observed. In daily scintillation activity occurs approximately one hour after sunset.

2.2.2 Solar cycle variations

The long-term variation in sunspot occurrence has a profound effect on the noon electron distribution. In the Figure 2.3, solar minimum shows that the scintillation maximizes at the peak of the equatorial anomaly rather than at geomagnetic equator.

The solar sunspot cycle is concerted with annual scintillation activity, which varies in every 11-year cycle as shown in Figure 2.4. That presents the solar cycles 22-23. The red line (1) is the monthly smoothed sunspot number while the blue line (2) is actual monthly sunspot number. Cycle 22 started in September 1986 and Cycle 23 started in May 1996 with the monthly SSN at 8.0 and peaked in April 2000 at 120.8. The last smoothed monthly sunspot number is for August 2003 at 60.0 [4].

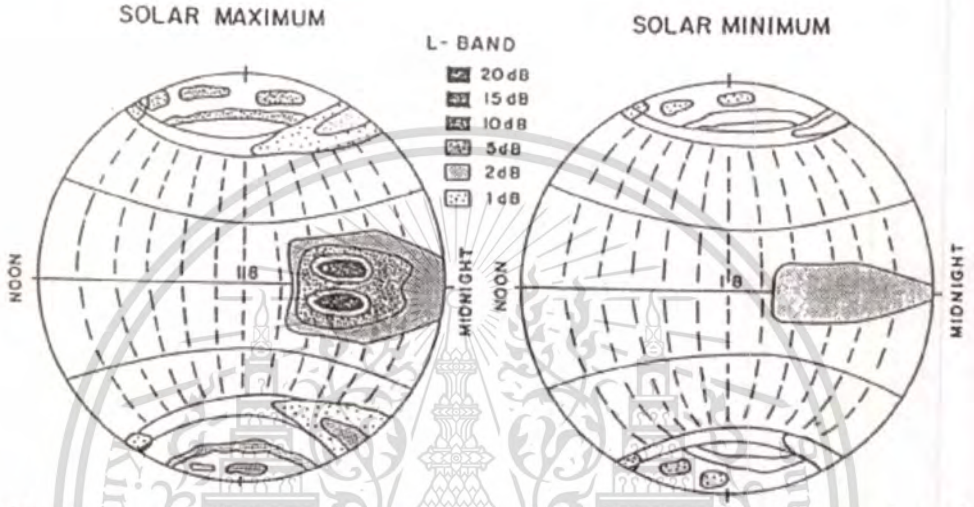

Figure 2.3 Fading depth of scintillation at L-band during low and high sunspot number.

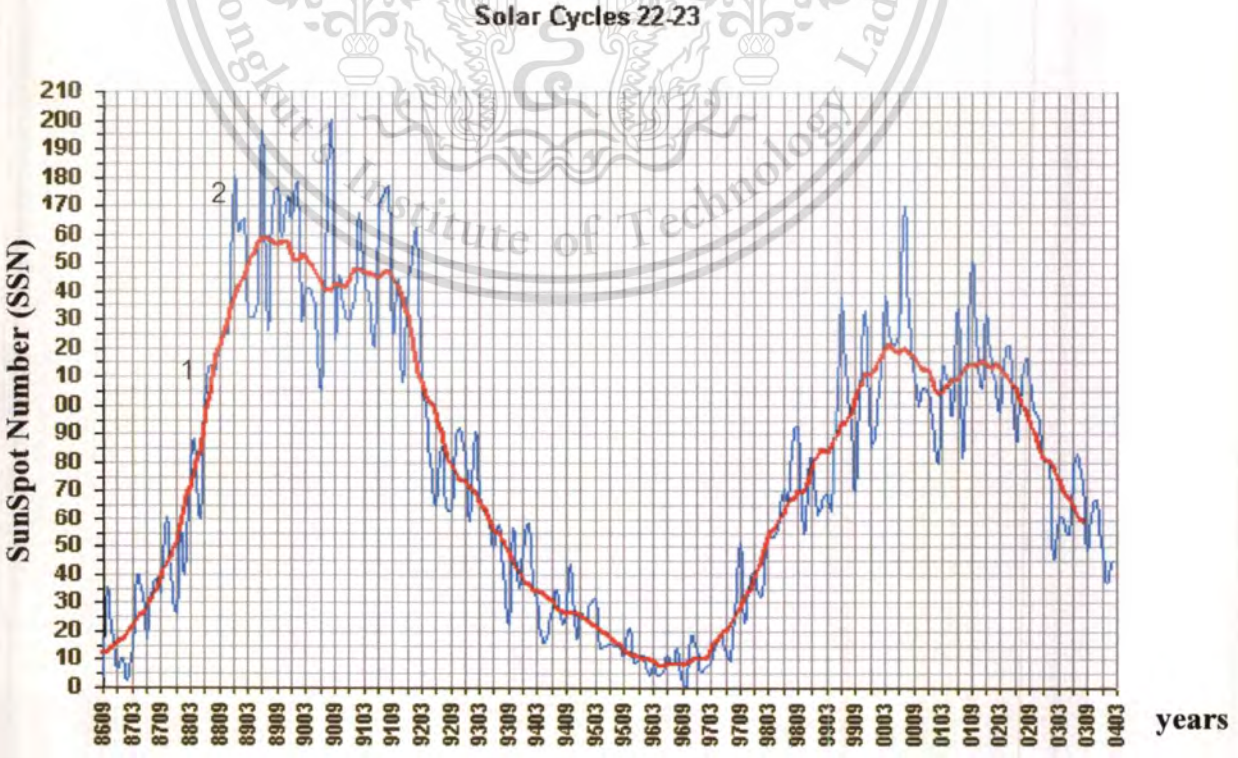

Figure 2.4 The Solar cycle in years 1986 –2004

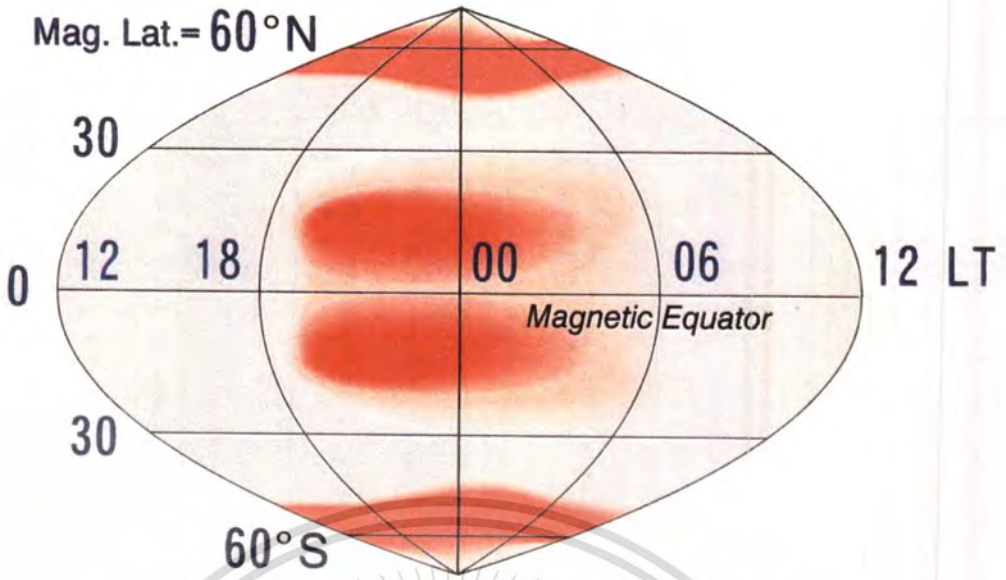

Figure 2.5 Scintillation distribution

2.2.3 Geographical variations

From Figure 2.5, it is shown that schematically the latitudes and times in which scintillation occurs [5]. There are two regions of ionospheric scintillation intensity. One region is the anomaly region of the equatorial ionosphere, which shows the most of intense scintillation, the high latitude. Gigahertz ionospheric scintillation of any significant amplitude only occurs within approximately $\pm 20^{\circ}$ of the magnetic equator for geostationary communications satellite links.

2.2.4 Frequency variation

Characteristics of the irregularities also affect scintillation frequency characteristics. Therefore the high frequency and the intensity of ionospheric scintillation will be weaker. The frequency dependence can be determined by relating the ratio of amount of power in the scintillating component (measured by S_4 index) to the frequency ratio. The frequency dependence becomes less steep for strong scintillation, as S_4 approaches a maximum value near unity with a few raw exception when S_4 exceeds 0.6 the frequency dependence exponent decrease [6].

2.3 Scintillation Index S_4

In the initial stages of scintillation research, when the usage of chart recording systems was common, other scintillation indices were used. The highly subjective nature of the classification systems such as the S.I. value made comparisons between data sets obtained by different research efforts very difficult. Following the series of different indices are suggested, workers in the field settled on the S_4 index to be the standard as it provides the unambiguous definition and it is easily computed using modem techniques. The S_4 index is used in several different contexts in the scintillation research field. Its usage to grade the severity of measured scintillation has already been mentioned.

The scintillation index S_4 is related to the peak-to-peak fluctuations of the intensity. The intensity scintillation is characterized by the variance in received power with the S_4 index commonly used for intensity scintillation and defined as the square root of the variance of received power divided by the mean value of the received power [7].

$$S_4 = \frac{\sigma_x}{m_x} \tag{2.1}$$

where σ_x is standard deviation and m_x is a mean value.

When used in this manner, investigators have determined that there are a couple of levels of scintillation, described by

- weak scintillation for $S_4 < 0.6$
- strong scintillation for $S_4 > 0.6$
- saturation for $S_4 > 1.0$

The importance of the three cases lies on the analysis of the scintillation behavior and the level of disruption to communications. Obviously, when the signal reaches to saturation, information content is usually lost. The weak and strong case distinctions are tied to the applicability of the propagation models used in analyzing the effect of the electron density irregularities on the transionospheric signal. The empirical relationship between S_4 index and the approximate peak-to-peak fluctuations $P_{fluc}(\mathrm{dB})$ as indicate in equation (2.2) [8]

$$P_{fluc} = 27.5 S_4^{1.26} \tag{2.2}$$

From equation (2.2) provides a convenient conversion between S_4 and $P_{fluc}(\text{dB})$ as present in Table 2.1

Table 2.1 Empirical conversion between S_4 index and $P_{fluc}(\text{dB})$

S_4	$P_{fluc}(\text{dB})$
0.1	1.5
0.2	3.5
0.3	6
0.4	8.5
0.5	11
0.6	14
0.7	17
0.8	20
0.9	24
1.0	27.5

2.4 Conclusion

This chapter presents the theory and factor of ionospheric scintillation variation. Before discussing in the next chapter, it is useful to outline the various parameters, which is the characteristic of ionospheric scintillation. Therefore the variation of scintillation is depending on many factors, such as time, position and frequency. The scintillation occurrence and their intensity increase maximum during equinoctial month and secondary maximum during solstice. In addition to the equatorial region is known that the higher scintillation. Finally, the scintillation index S_4 is related to the intensity of amplitude scintillation.

CHAPTER 3

EXPERIMENTAL SYSTEM AND AMPLITUDE DISTRIBUTION IN SHORT-TERM

Details of measurement system and analysis of amplitude distribution in short-term are presented in this chapter. The statistical analysis of amplitude scintillation distribution presents the probability density function (pdf) and cumulative density function (cdf) of Gaussian Nakagami-m distribution compared with experiment results of new model. The experiment on radio wave transmission at Bangkok, Chiang Mai and Cholburi are conducted in equatorial regions that having a great amount of scintillation activity.

3.1 Experiment system

The experimental system of ionospheric scintillation is observed on VHF Signal, S-band and C-band. For VHF, we received 244.165 MHz from FLTSATCOM (Fleet Satellite Communications) at Bangkok station (KMITL), since October 2002 to December 2003. The signal was received by yagi-uda 9 elements and the elevation angle of the link is 52.15°. For the experimental results of amplitude scintillation on S-band receiving station has been installed at Bangkok (KMITL) and Chiang Mai (CMU: Chiang Mai University) received 1.694 GHz carrier wave of a telemetry signal from the stationary GMS-5 satellite (Geostationary Meteorological Satellite-5) at 140 °E for both stations. The parabolic receiving antenna has 1.8-meters diameter. The measurements are started on January 2000 to December 2003 and February 2000 to July 2003 for KMITL and CMU respectively. The processing data system of VHF and S-band at KMITL consist of a data-collecting computer that samples an analog signal from the receiving system at 50Hz (0.02s). For CMU station (S-band), the database of amplitude scintillation will access via Internet by sampling from original data (50Hz) every 10s (0.1Hz). Block diagrams of VHF and S-band are presented in Figure 3.1.

Moreover on C-band scintillation, the observation stations at Cholburi, Sriracha received the satellite beacon signal at 3.9525 GHz and 3.9475 GHz from INTELSAT 802,

INTELSAT 904 satellite over the Pacific Ocean Region (POR) at 174° E from January-December 2002 and the Indian Ocean Region (IOR) at 60° E from July-December 2002 respectively. The satellite beacon signal is down converted to an intermediate frequency (IF) of 70 MHz. Furthermore, data is sampled every 1s, block diagram of this station as show in Figure 3.2. The propagation geometry for each station is presented in Table 3.1. Which summarizes the parameters related to the satellite signal reception for each station.

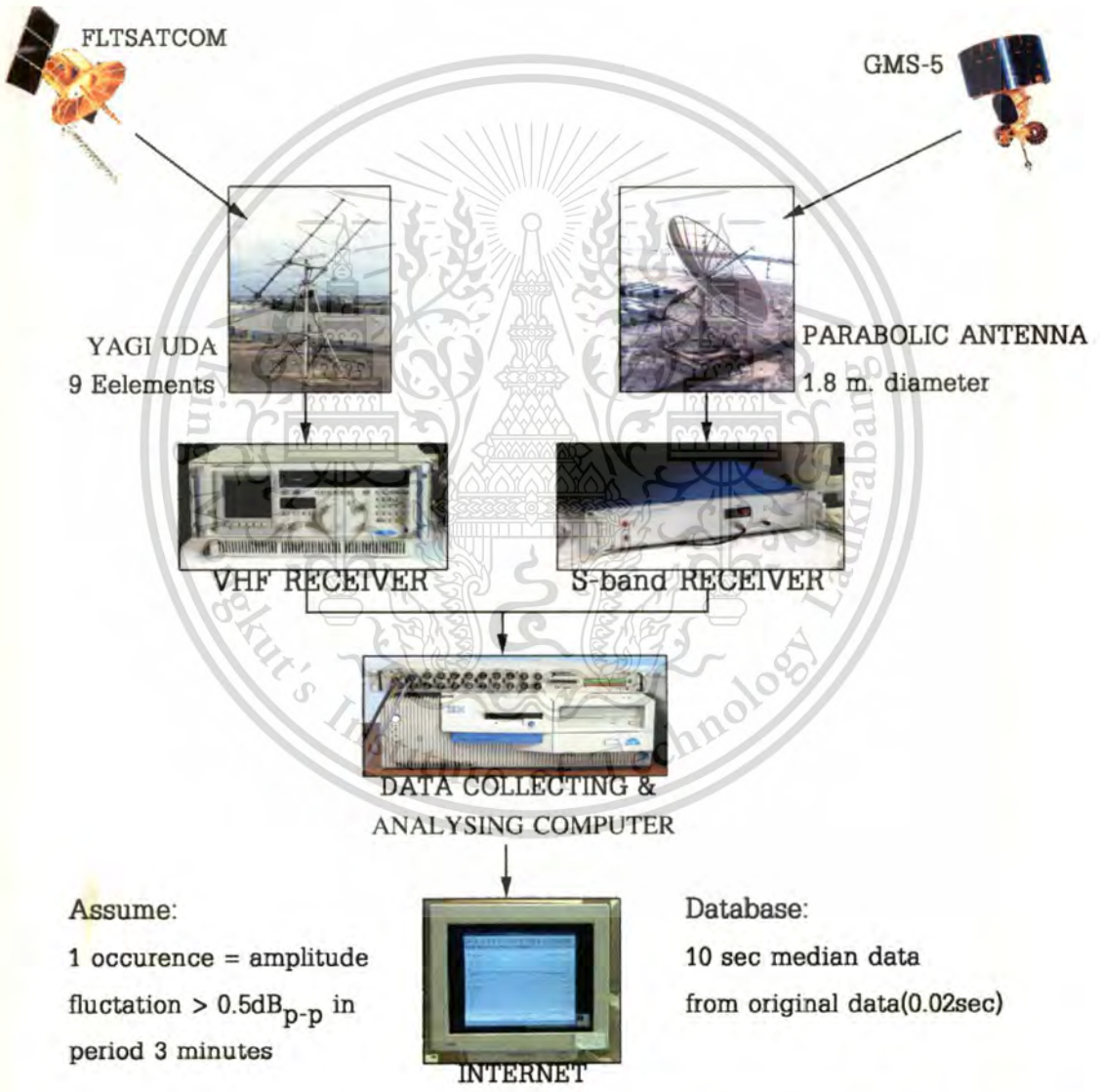

Figure 3.1 Block diagram of VHF signal and S-band observation system

In this thesis analyzes the scintillation data at the position around magnetic equator the area is the most intense fading is observed most frequency, especially

S-band measurement during years of solar maximum. For analysis the modeling of amplitude distribution in short-term, this thesis chose VHF because the amplitude scintillation can be observed maximum. S-band scintillation was considered at KMILT (2.8° N Geomagnetic latitude) and CMU (7.9° N Geomagnetic latitude) that the CMU station is near the equatorial anomaly. In addition, C-band is high frequency signal while amplitude scintillation will be minimal. Therefore, these frequencies are variety to analyze model in short-term amplitude scintillation. We can regard the scintillation event when amplitude scintillation fluctuate exceed 0.5 dB_{p-p} in time period 3 minutes, which is counted for one scintillation occurrence.

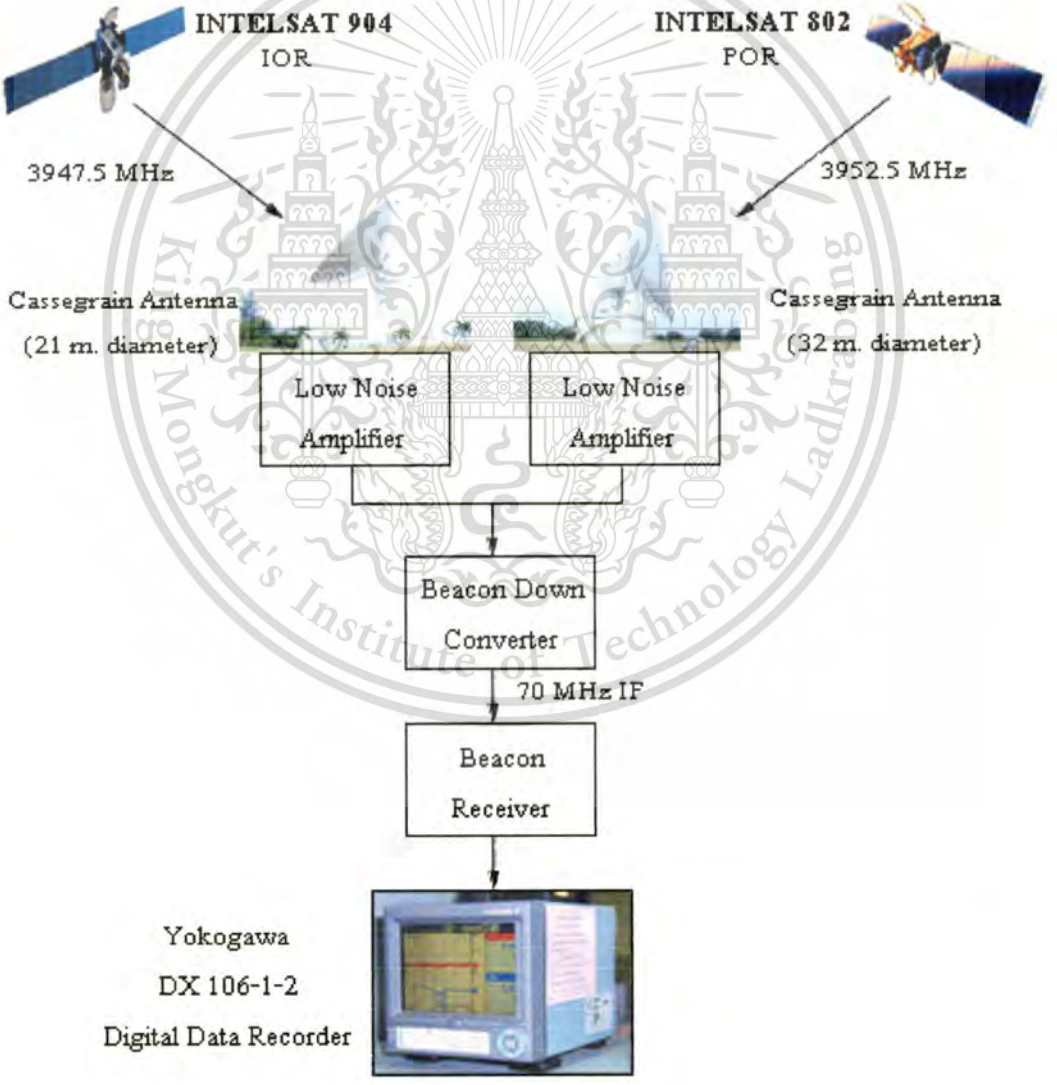

Figure 3.2 Block diagram of C-band at Sriracha, Cholburi

For statistic in long-term scintillation has been analyzed by using 10s sampling from original data. The first step of data analysis was to clean up the background system noise by using a high-pass filter. A data selection was made of 30 days of measurement in every year of experiment. From each month of years, at least one day was selected. Segments of these events were selected for detailed statistical analysis. The segments of scintillation data were chosen from different seasons and different strengths. Especially, data of scintillation pronounced in strong scintillation, most of the days were always selected in the summer months. Approximately 250 events were analyzed.

Table 3.1 Satellite receiving station parameters

Frequency Band	VHF	S-band		C-band	
Frequency	244.165 MHz	1.694 GHz		3.9475 GHz	3.9525 GHz
Satellite	FLTSATCOM	GSM-5		INTELSAT 904 (IOR)	INTELSAT 802 (POR)
Position	100.8°E, 13.7°N (Bangkok)	100.8°E, 13.7°N (Bangkok)	99.0°E, 18.8°N (Chiang Mai)	13° 06' N , 100° 56' E (Cholburi at Sriracha)	
Satellite Position	71 °E	140 °E		60° E	174° E
Elevation angle	52.15°	42.40°	38.84°	40°	8°
Azimuth angle	247.53°	106.2°	110.34°	255.2°	93.96°
Antenna	Yagi Uda, 9 element	1.8 m.		21 m.	32 m.
Polarization	RHPC	Linear Polarization		RHPC	
Period of scintillation observation	10/2002 to 12/2003	01/2000 to 12/2003	02/2000-07/2003	06/2002 to 12/2002	01/2002 to 12/2002

3.2 Analysis of Scintillation Intensity

Scintillation Index S_4 is one of the most important parameters in the ionospheric scintillation. This thesis uses S_4 index measures the severity of the intensity of amplitude scintillation. The parameter S_4 can be averaged over any appropriate periods. Figure 3.3 presents the amplitude scintillation event at KMITL station on S-band compares with S_4 index that is calculating every 1-minute and 5-minute. From Figure 3.3 can be observed that S_4 index was corresponding with amplitude scintillation on 14 September 2002.

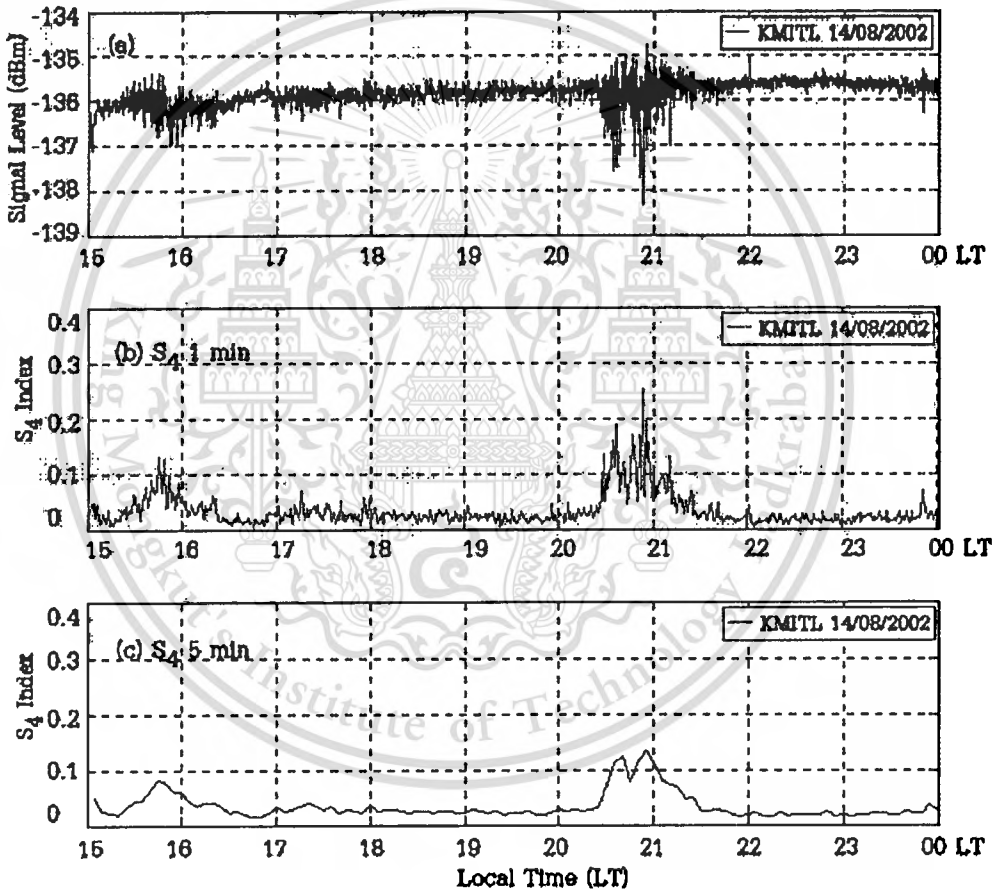

Figure 3.3 Comparison between amplitude scintillation intensity and level of S_4 index

From Figure 3.3c can see the S_4 level is decrease when calculated in 5-minutes. The time shifts between amplitude fluctuation peaks and S_4 index can be observed in Figure 3.3b and 3.3c. However, statistical analysis in short-term is calculated in period 5-minutes as mentioned in the next section.

3.3 Amplitude Distribution in Short-term

To study the probability distributions of the scintillation signal theoretically, several approaches have been adopted in the literature. Normally, it is known that the theoretical and experimental investigations which are the probability density of short-term amplitude scintillation following a Gaussian distribution and Nakagami-m distribution. However, it has been found that for strong scintillation intensities, the short-term distribution is not as symmetrical as the Gaussian distribution. Although Nakagami-m distribution is suitable more than Gaussian distribution but it is close to amplitude scintillation only large fade. Therefore this chapter is to analyze and design modeling of amplitude scintillation in short-term for every situation. Knowledge of the probability density function (pdf) of amplitude scintillation is essential if one is to obtain the overall satellite link availability [9].

3.3.1 Amplitude Scintillation Probability Density Function

The change of irregularities medium in ionosphere caused of amplitude scintillation comprise random process is nonstationary. It is considered under condition of stationary process if the irregularities condition is not changing in during period, which is short enough to remain constant. It can be described in short-term pdf, which exists during these intervals of stationary (i.e., constant scintillation intensity σ_x). In generally, it is described either by a probability density function or cumulative distribution function.

3.3.1.1 Gaussian or Normal Distribution

This distribution is applied to a continuous variable of any sign. The probability density function as [2]:

$$p(x) = \frac{1}{\sigma\sqrt{2\pi}} \exp\left(-\frac{1}{2}\left(\frac{x-m}{\sigma} \right)^2 \right) \tag{3.1}$$

where m is mean value, and σ is standard deviation.

for cumulative density function as:

$$F(x) = \frac{1}{\sigma\sqrt{2\pi}} \int_{-\infty}^{x} \exp\left(-\frac{1}{2}\left(\frac{t-m}{\sigma} \right)^2 \right) dt = \frac{1}{2}\left(1 + erf\left(\frac{x-m}{\sigma\sqrt{2}} \right) \right) \tag{3.2}$$

3.3.1.2 Nakagami-m Distribution

This distribution is applied to a non-limited positive variable. The probability density function is equal to:

$$p(x) = \frac{2m^m}{\Gamma(m)\Omega^m} x^{2m-1} e^{-\frac{m}{\Omega}x^2} \tag{3.3}$$

where Ω is a scale parameter equal to the mean value of x^2 and the parameter m is equal to the inverse square of scintillation index S_4.

$$m = \left(\frac{\Omega}{x^2 - \Omega} \right)^2 = \frac{1}{S_4^2} \geq \frac{1}{2} \tag{3.4}$$

The cumulative density function of Nakagami-m is close form expression as

$$F(x) = \int_0^x p(x)dt = \frac{\Gamma(m, mI)}{\Gamma(m)} \tag{3.5}$$

where $\Gamma(m, mI)$ is the incomplete gamma function and $\Gamma(m)$ is gamma function.

3.3.1.3 New model (Modified by Viparat Torchakul)

This model is applied from nonlinear regression and Bayes' theorem. From the law of total probability can be use to derive an important formula called Bayes' Formula, the analysis of new model presents in appendix A. New model separated the level of intensity by S_4 index, as shown in Table 3.2.

Therefore, the probability density function of new model in case S_4<0.5 can be written as:

$$nm(x) = \frac{1}{p} \exp\left(\frac{-2.25v_i}{\sigma^{3/2}}(x-m)^2 - \frac{5}{2m_1^{\sigma}}(x-m) - \left[\frac{4.3-0.7\log\sigma^2}{5}\right]\left[\sqrt{\sigma} + \log\sigma^2\right]\right) \tag{3.6}$$

p is the total of probability, m is mean value and m_1 is equal to the inverse square of scintillation index S_4. (m_1 is identical with m of Nakagami-distribution)

$$p = \sum_{x=-\infty}^{\infty} \exp\left(\frac{-2.25v_i}{\sigma^{3/2}}(x-m)^2 - \frac{5}{2m_1^{\sigma}}(x-m) - \left[\frac{4.3-0.7\log\sigma^2}{5}\right]\left[\sqrt{\sigma} + \log\sigma^2\right]\right) \tag{3.7}$$

Table 3.2 The level of S_4 index analyzes in new model

i	S_4 index level	v_i	Parameter in second term
1	S_4<0.9	$\frac{2.3}{18}$	$\frac{2.25}{10.5\sigma^{3/2}}$
2	0.8< S_4 <0.9	$\frac{1}{14}\left(\frac{7.5S_4+2.5\sigma}{3.75\sqrt{S_4\cdot\sigma}}-0.2\sqrt{\sigma}\right)$	
3	0.7< S_4 <0.8	$\frac{1}{16}\left(\frac{7.5S_4+2.5\sigma}{3.75\sqrt{S_4\cdot\sigma}}\right)$	
4	0.5< S_4 <0.7	$\frac{1}{13}\left(\frac{\sigma+\sqrt{S_4}}{2}\right)$	
5	0.4< S_4 <0.5	$\frac{1}{13}\left(\frac{5}{2}\sqrt{S_4}+1\right)$	$\frac{5}{2m_1^{\sigma}}$
6	0.2< S_4 <0.4	$\frac{1}{10.5}\left(\frac{2+S_4}{2\sqrt{S_4}}\right)$	
7	0.15< S_4 <0.2	$\frac{1}{9.5}\left(\frac{1}{2\sigma}+0.85\sqrt{\sigma}+\frac{1}{\sqrt{\sigma}}\right)$	
8	S_4<0.15	$\frac{1}{9}\left(\frac{1}{\sigma}+2\sqrt{S_4}\right)$	

In case S_4>0.5; the probability density function of new model as

$$nm(x)=\frac{1}{p}\exp\left(\frac{-2.25v_i}{\sigma^{3/2}}(x-m)^2-\frac{2.25}{10.5\sigma^{3/2}}(x-m)-\left[\frac{4.3-0.7\log\sigma^2}{5}\right]\left[\sqrt{\sigma}+\log\sigma^2\right]\right) \quad (3.8)$$

and

$$p=\sum_{x=-\infty}^{\infty}\exp\left(\frac{-2.25v_i}{\sigma^{3/2}}(x-m)^2-\frac{2.25}{10.5\sigma^{3/2}}(x-m)-\left[\frac{4.3-0.7\log\sigma^2}{5}\right]\left[\sqrt{\sigma}+\log\sigma^2\right]\right) \quad (3.9)$$

Hence, the cumulative distribution function of new model can be express

$$F(x)=\int_{-\infty}^{x} nm(x)dx \quad (3.10)$$

The probability density functions of amplitude scintillations are indicated in Figure 3.4, 3.5 and 3.6. The theory of the Gaussian distribution, Nakagami-m distribution and new model are compared to the experiment of amplitude scintillation in short-term.

In Figure 3.4, 3.5 and 3.6, are presented the result of short-term amplitude scintillation distribution on C-band, S-band (KMITL and CMU) and VHF respectively. In order to obtain a statistically reliable value of σ_x, and must be short enough for the irregularities medium to remain reasonably constant, therefor 5-10 minutes have been possible as suitable [10].

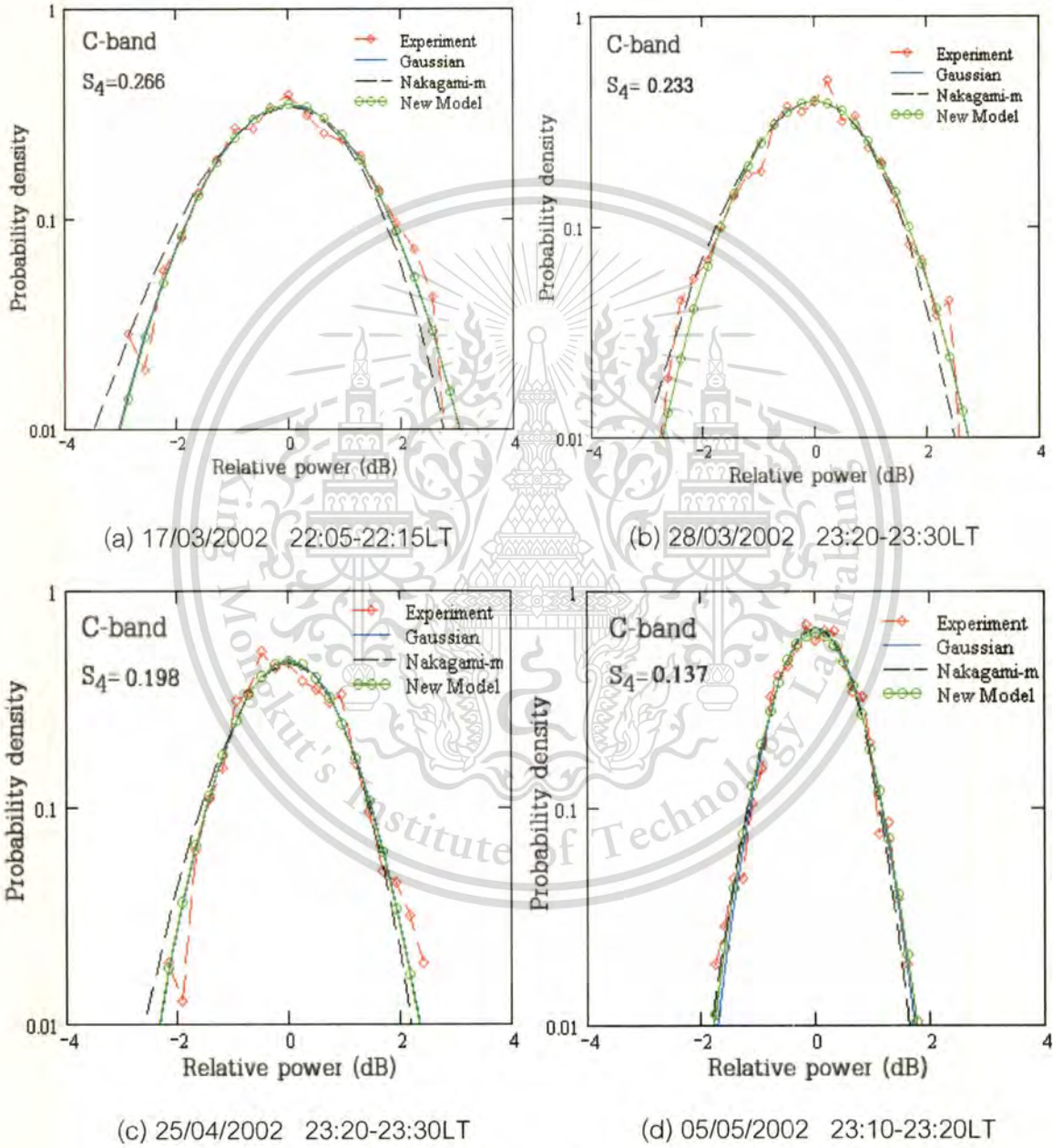

Figure 3.4 probability density functions of amplitude scintillations in C-band

Figure 3.4a-d presents the C-band scintillation in short-term, for weak and strong scintillation by Gaussian, Nakagami-m distribution and new model. In Figure can be

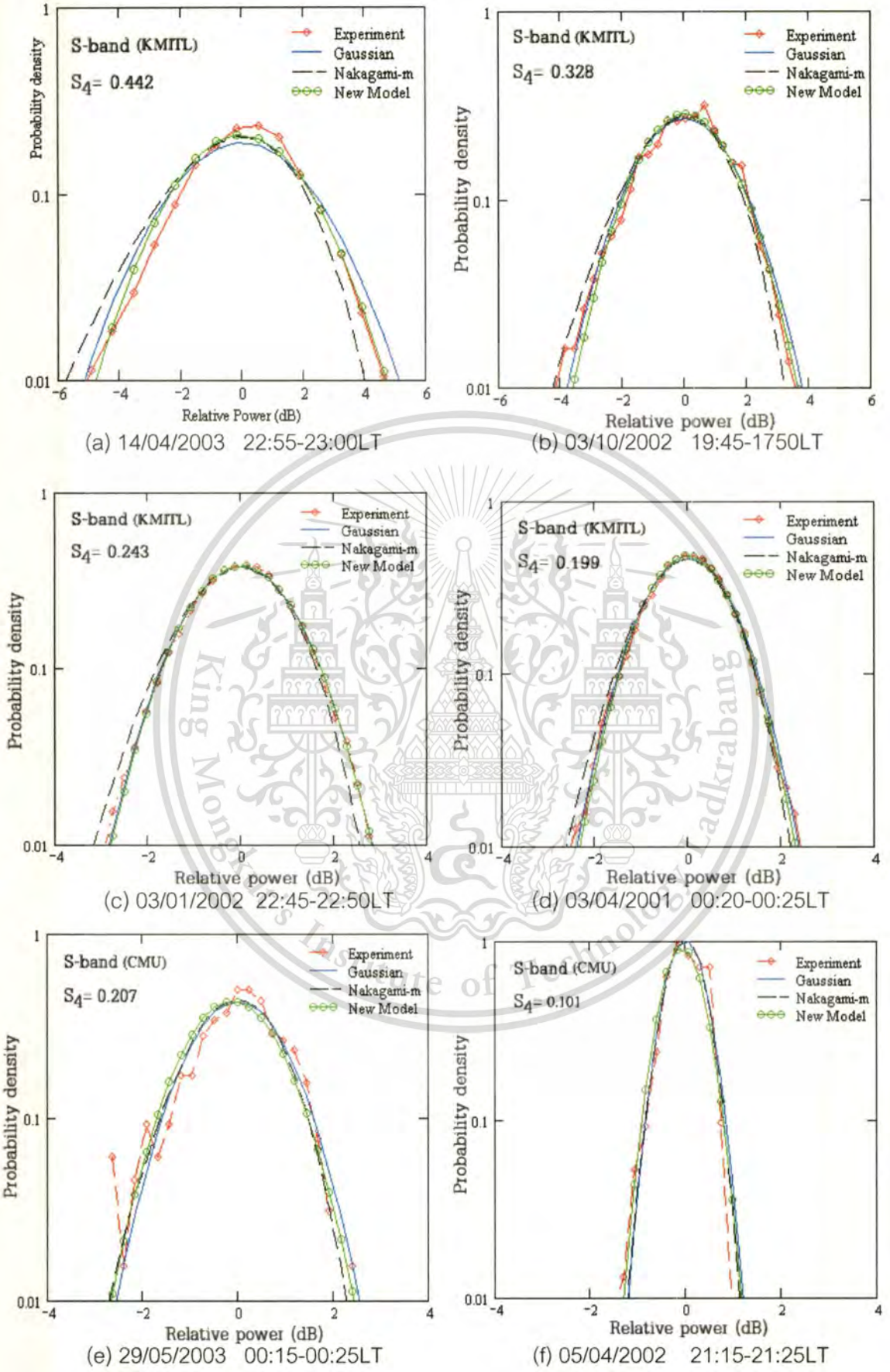

Figure 3.5 probability density functions of amplitude scintillations in S-band

found the new model is similar to Gaussian distribution. For small fluctuation (Figure 3.4d), there were little difference between Gaussian, Nakagami-m distribution and new model. Thus, weak scintillation can present equally well by these models. Even though some events have correlation coefficient of new model (in Table 3.3) less than Gaussian; however, the new model is reasonable to use in short-term because the percentage of the correlation coefficient of experiment results and new model is more than Gaussian distribution, as shown in Figure 3.7a.

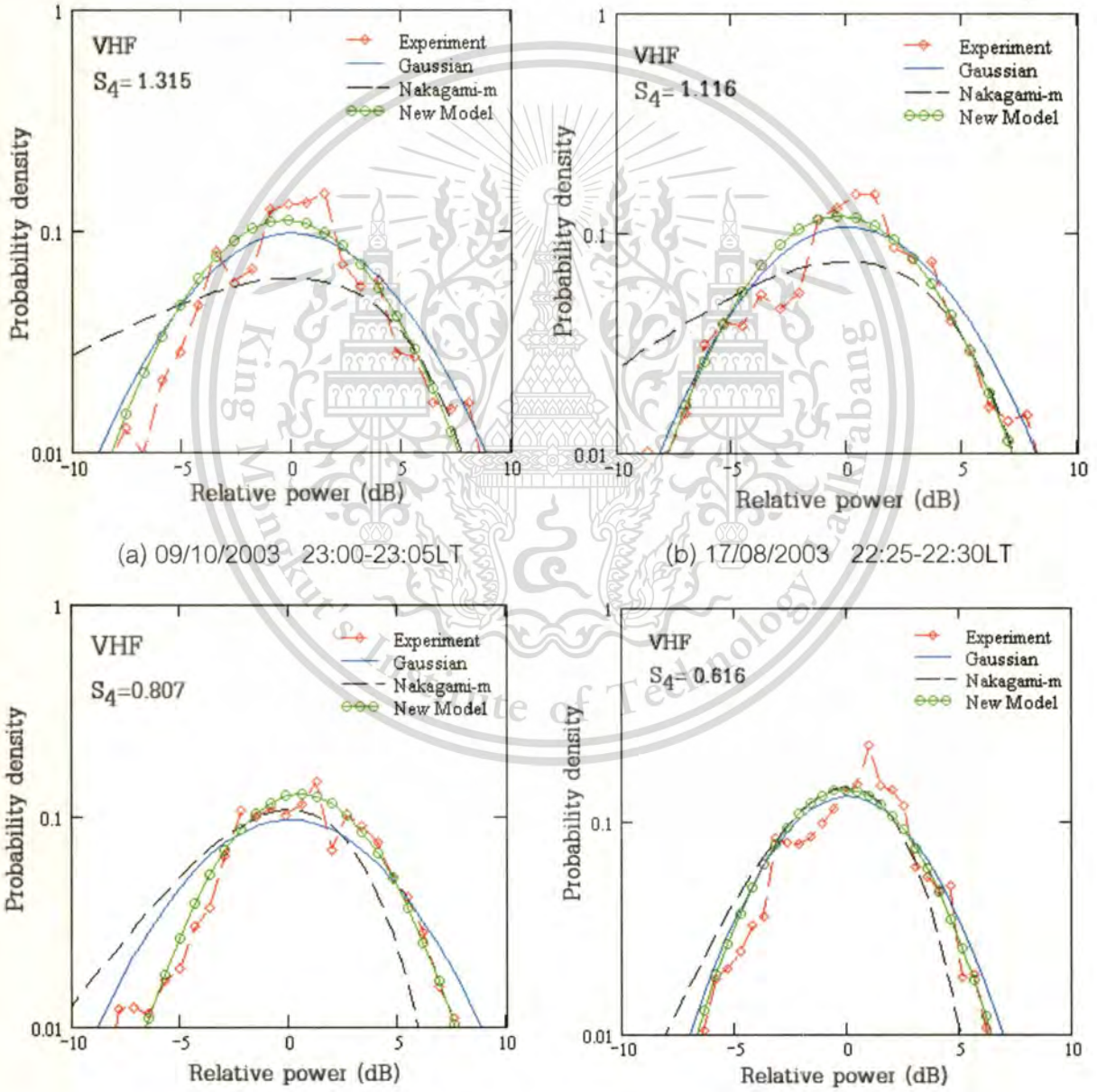

Figure 3.6 probability density functions of amplitude scintillations in VHF

From Figures 3.5 a-f, it can be seen that the new model is suitable for the large enhancement more than Gaussian distribution and some events the new model is close to the large fade more than Nakagami-m distribution. From Figure 3.5e-f as show the amplitude scintillation at CMU station, that the new model is consistent with experiment results. The amplitude scintillation at CMU calculated in during 10 minutes caused by the data is sampling 10s while amplitude scintillation at KMITL analyze in 5-minutes and the data is sampling 0.02s. In addition to VHF scintillation, in Figure 3.6a-d seen the Nakagami-m distribution is not close to the large fade when S_4 index is higher. From these Figures, the new model appears suitably with experiment more than Gaussian and Nakagami-m distribution, when strong scintillation. The amplitude scintillation in Figure 3.6(a) is shown the level of S_4 index is highest and the new model is remaining close to the experiment results more than other models. To verify the new model, it can be used in another area and some data of amplitude scintillation observations made from middle latitude in Yamagawa, Japan at 1.694 GHz (S-band) are analyzed as shown in Figure 3.7a and 3.7b. That can be seen in the Figure, the new model is also close to large fade and enhancement.

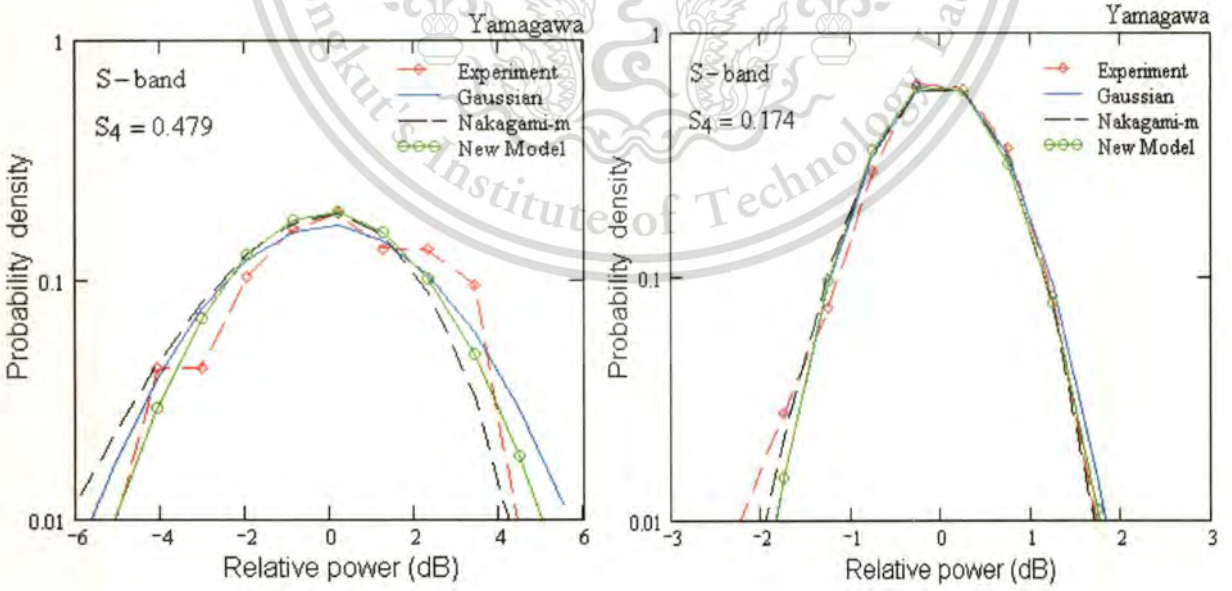

(a) 30/05/2001 23:30-23:40LT (b) 08/08/2002 01:10-01:20LT

Figure 3.7 probability density functions of amplitude scintillations at Yamagawa.

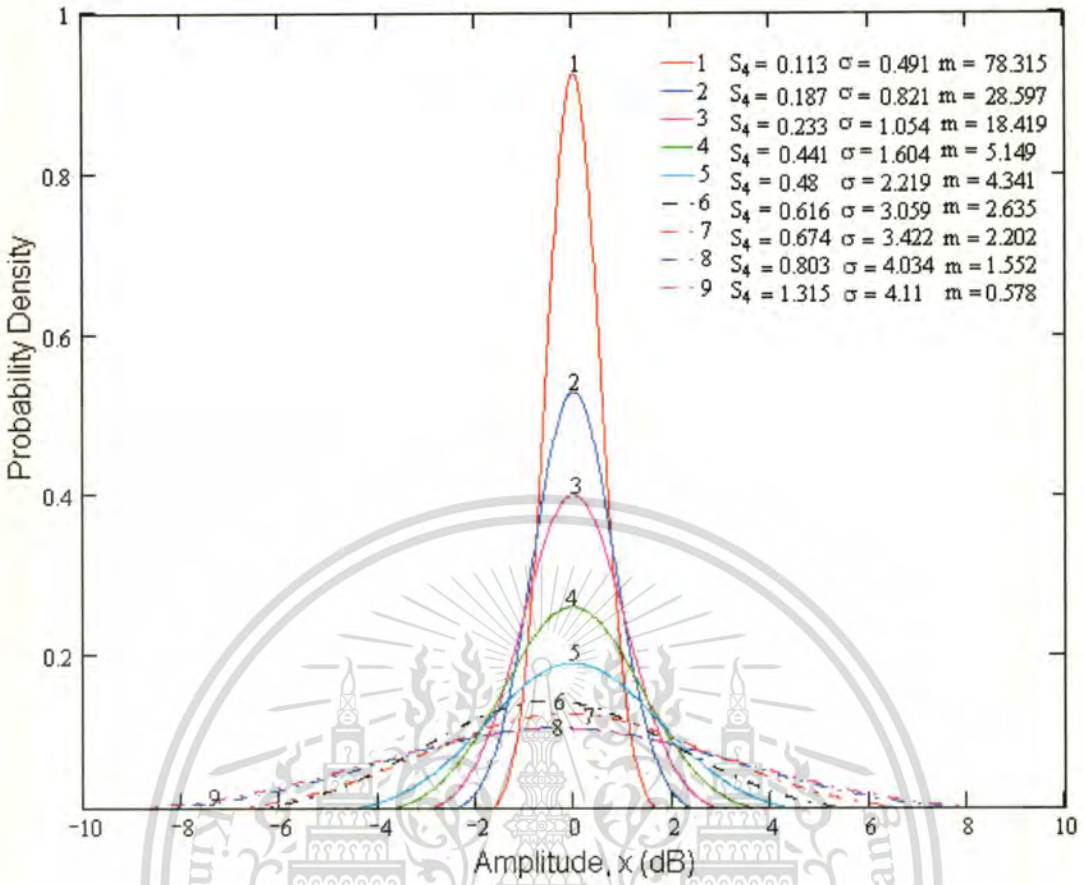

Figure 3.8 Probability density function of signal level of x for value from experiment

Figure 3.8 shows that the distribution function of new model, for different values of the parameter S_4 index. This Figure clearly shows that the S_4 index is increase, while the model is decrease and spread in fade side.

In addition to assess the strength of dependence between two random variables (between experiment and model), that is through their correlation coefficient for presented the relative between experiment and these models. The correlation coefficient of experiment results from Figure 3.4-3.7 as show in Table 3.3. The percentage of correlation coefficient between these models are show in Figure 3.9 and the analysis of the correlation coefficient are described in appendix B. In Figure 3.9(a), (b) and (c) compare with Gaussian distribution and new model on C-band, S-band and VHF respectively. From Figure 3.9b, the results of new model on S-band have a correlation coefficient with experiment results more than C-band and VHF.

Figure 3.9 Percentage of the correlation coefficient between Experiment distribution and new model versus between Experiment distribution and Gaussian distribution. (a) The percentage of the correlation coeff. in C-band (b) The percentage of the correlation coeff. in S-band and (c) The percentage of the correlation coeff. in VHF

The Percentage of correlation coeff. between Experiment and new model more than Gaussian

The Percentage of correlation coeff. between Experiment and Gaussian more than new model

The Percentage of correlation coeff. between Experiment and new model equal to Gaussian

The Percentage of correlation coeff. between Experiment and new model equal to Nakagami-m

Table 3.3 The correlation coeff. between Experiment result and new model and Gaussian

Frequency	Scintillation events	S_4 index	The correlation coeff. between experiment results and	
			new model	Gaussian
C-band	(a) 17/03/02 22:05-22:15LT	0.266	0.99	0.991
	(b) 28/03/02 23:20-23:30LT	0.233	0.972	0.97
	(c) 25/04/02 23:20-23:30LT	0.198	0.975	0.974
	(d) 05/05/02 23:10-23:20LT	0.137	0.99	0.99
S-band	(a) 14/04/03 22:55-23:00LT	0.674	0.992	0.972
	(b) 03/10/02 19:45-1750LT	0.442	0.99	0.974
	(c) 03/01/02 22:45-22:50LT	0.237	0.999	0.998
	(d) 03/04/01 00:20-00:25LT	0.199	0.998	0.998
	(e) 29/05/03 00:15-00:25LT	0.207	0.971	0.971
	(f) 05/04/02 21:15-21:25LT	0.101	0.973	0.971
VHF	(a) 09/10/03 23:00-23:05LT	1.315	0.962	0.935
	(b) 17/08/03 22:25-22:30LT	1.116	0.969	0.947
	(c) 24/10/03 23:15-23:20LT	0.807	0.974	0.946
	(d) 14/10/02 01:35-01:40LT	0.616	0.959	0.935
S-band at Yamagawa	(a) 30/05/01 23:30-23:40LT	0.479	0.964	0.961
	(b) 08/08/02 01:10-01:20LT	0.147	0.996	0.994

3.3.2 Cumulative amplitude distribution function

Engineers designing the earth-space links must determine the fade margin necessary to overcome the degradation caused by scintillations, under various conditions of ionosphere. The cumulative amplitude distribution function (cdf), a first order statistics, is useful for defining the fade margin requirement for communication systems as it expresses the probability that the signal level exceed a given decibel level. Figure 3.10, 3.11 and 3.12 are presented the cumulative amplitude distribution function that can be obtain from some events of probability density function in Figure 3.4-3.6 respectively.

For cumulative amplitude distribution function of scintillation samples is shown that one strong and one weak, with S_4 index in each frequency. In Figure 3.10-3.12, it can be found the cdf, which there is strong correlation between the depth fade and peak enhancements with increasing S_4 index. The level of scintillations which is particular interesting to a system engineer and can be read from the cdf that is the peak enhancement, maximum fade, 5% peak and 95% fade. These statistical signal levels in decibels corresponding to the cdf in Figure 3.10-3.12 are given in Table 3.4.

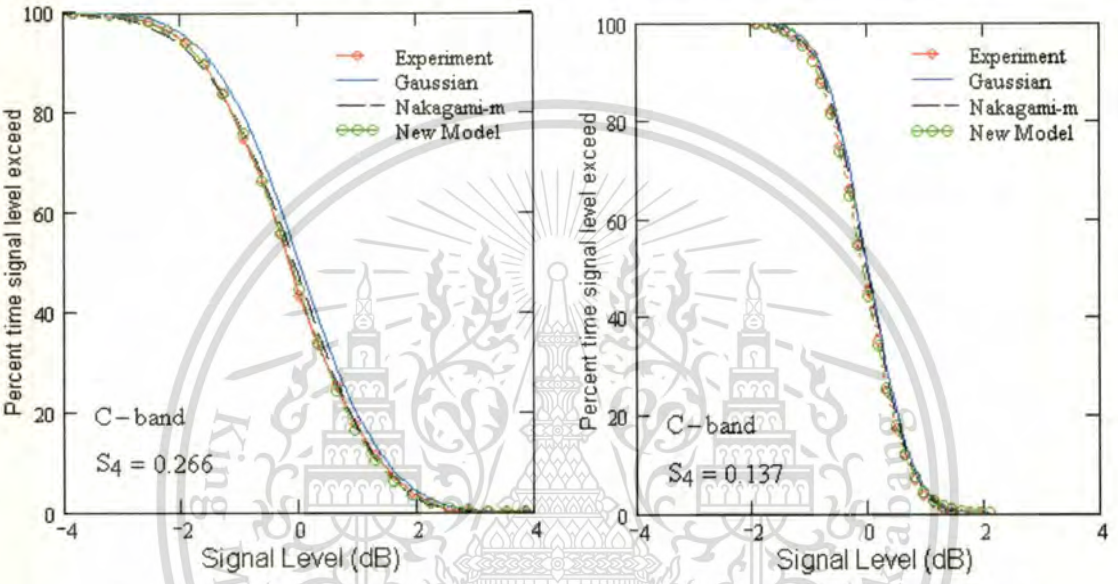

(a) 17/03/2002 22:05-22:15LT (b) 05/05/2002 23:10-23:10 LT

Figure 3.10 The cumulative amplitude distribution function in C-band

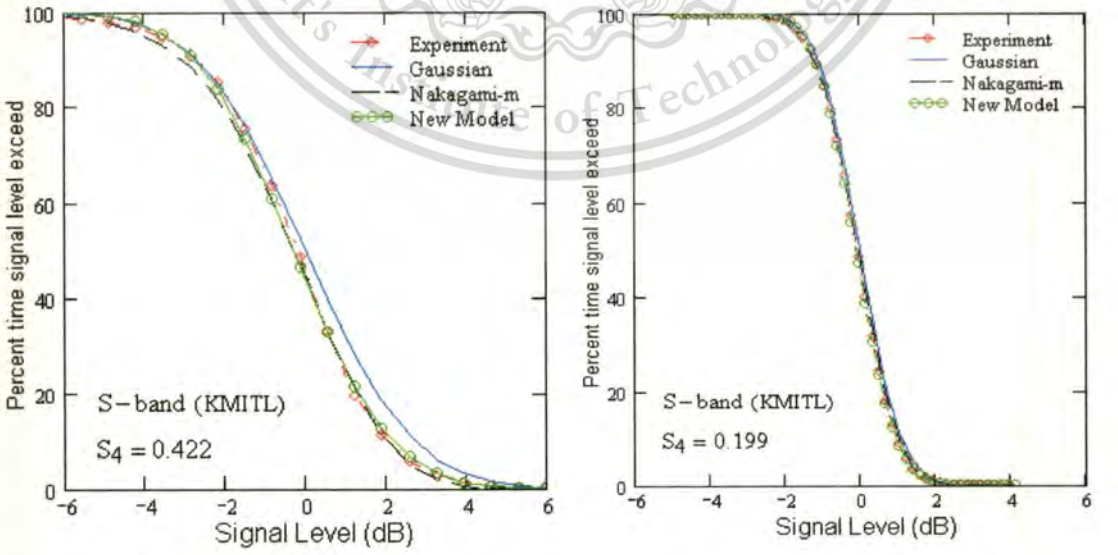

(a) 14/04/2003 22:55-23:00LT (b) 22/08/2000 21:40-21:45LT

Figure 3.11 The cumulative amplitude distribution function in S-band

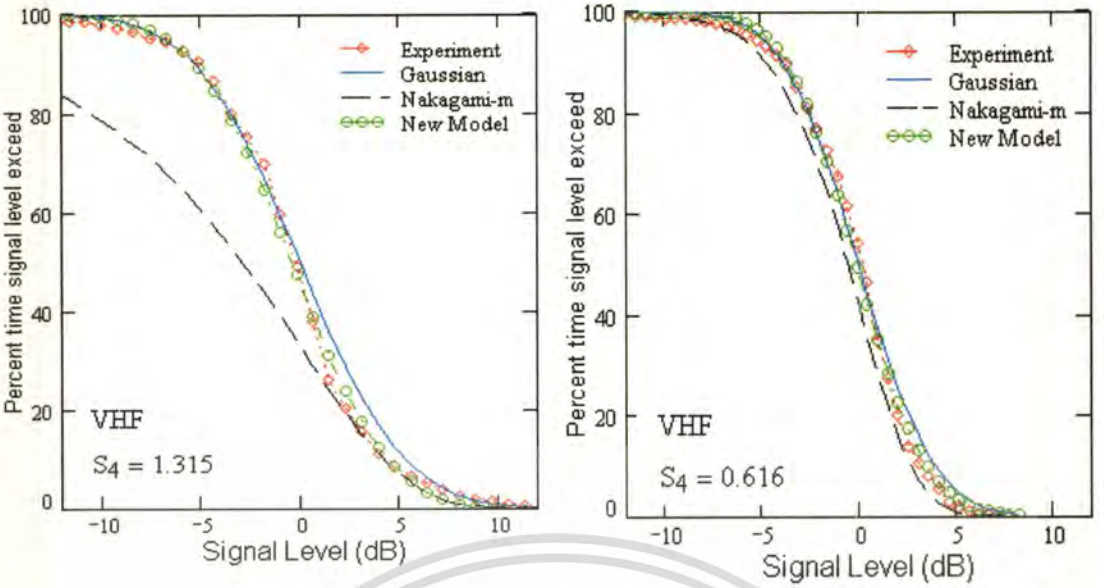

(a) 15/10/2002 02:35-02:40LT (b) 09/10/2003 23:00-23:05LT

Figure 3.12 The cumulative amplitude distribution function in VHF

Table 3.4 Cumulative distribution function statistics

Frequency	S_4 index	Peak Enhancement (dB)	Maximum Fade (dB)	5% Peak (dB)	95% Fade (dB)
C-band	0.266	3.43	-3.82	1.85	-2.01
	0.137	2	-1.9	0.85	-0.9
S-band	0.442	6.78	-11.80	2.65	-3.72
	0.199	3.52	-3.86	1.23	-1.43
VHF	1.315	14.23	-20.08	6.54	-7.13
	0.616	6.94	-17.77	4.23	-5.55

Figure 3.10-3.12 presents the cumulative probability distribution of the ionospheric scintillations results. Also, theoretical of Nakagami-m, Gaussian distribution and new model were evaluated for comparisons with observe the cumulative distribution function. It is seen that the Gaussian distribution is a fit for the scintillation events with S_4 values less than 0.4 and Nakagami-m distribution is not appropriate with the amplitude scintillation when S_4 values more than 0.8. While new model appear suitably to the experiment results as S_4 values is higher. For the differences between 5% peak and

95% levels present the receiver dynamic range to be employed in a satellite system receiver [11].

3.5 Conclusion

This chapter is designed the model for predictable and observable trend of amplitude scintillation in short-term. For small fluctuation, there is small difference between Gaussian, Nakagami-m distribution and new model. Normally Gaussian distribution is appropriate for weak scintillation cases, whereas for Nakagami-m distribution appears suitably for both strong and weak scintillation. However, for strong scintillation, the new model is clearly corresponding to experimental results in these frequencies. Especially in the large enhancement can be observed the new model is coincides more than Gaussian distribution. Although, some events of new model are not close to the experiment, but in short-term amplitude scintillation the new model was found to be mostly suitable for VHF, S-band and C-band of experiment more than other distribution. It is describing scintillation fading, both weak and strong scintillation. For statistical analysis of amplitude scintillation results in short-term, it can see that the new model is quite appropriate for the scintillation events on S-band. The modeling of short-term amplitude scintillation is used for long-term amplitude scintillation. The modeling in long-term can determine the impacts on communication due to scintillation effect by using these scintillation model, such as determined the average probability of bit error.

For cumulative distribution function of amplitude scintillation can be obtained the difference value from 5% Peak and 95% fade. However all scintillation events calculation can obtain the average receiver dynamic ranges suitable to the scintillation characteristics in the particular station.

CHAPTER 4

MODELING IN LONG-TERM AND BINARY ERROR PROABILITY SUBJECT TO SCINTILLATION FADING

This chapter is primarily concerned with modeling of scintillation statistic in long-term, that compared with Gaussian distribution, Moulsley-Vilar distribution, analytical approximation and experimental results of new model in long-term. Considering the global fading process on earth-space link caused by amplitude scintillation, which is derived theoretical estimates of the average bit-error probability on a digital satellite link subject to scintillation fading.

4.1 Variation of Scintillation Intensity

As mentioned in previously, variation of irregularities medium along the path will affect the scintillation intensity. It means that the process cannot be considered strictly stationary in long term and this will have a significant impact on the statistics of the process [12]. Therefore, in any practical situation of the scintillation intensity (or σ_x) varies with time, due to changing of irregularities medium.

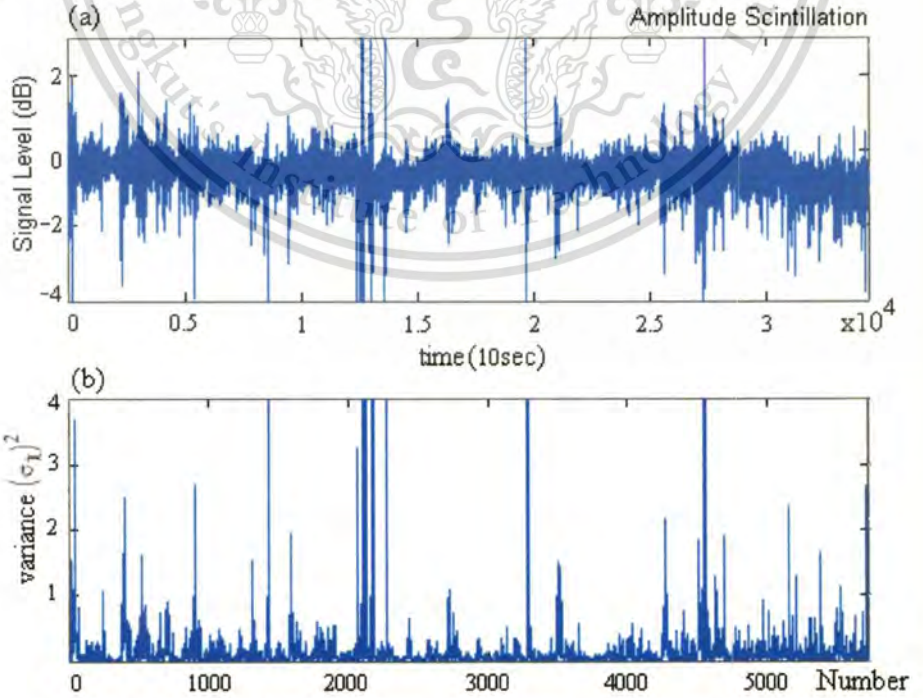

Figure 4.1 Comparison between amplitude scintillation and variance

For description the amplitude scintillation in long-term, we bring the data of amplitude scintillation arrange to continue and divide data in 1-minute period for calculated the variance every 1 minute. That can be seen the variation of variance along with amplitude scintillation as show in Figure 4.1a and 4.1b. From these variance can be obtained distribution in Figure 4.2a and 4.2b as curves 1 (red line). Our suitable data is following log-normal distribution: curve 2 (blue line). That curve is derived by log-normal distribution and experiment results of σ_x^2 (variance: in curve 1) are also shown the comparison. In Figure 4.2a and 4.2b present the amplitude scintillation at CMU station (S-band) and Cholburi station (C-band) in February-April 2000 and February-April 2002 respectively. It has been shown the information on the amplitude distribution of scintillation on a satellite path can be derived from the standard deviations of samples amplitude.

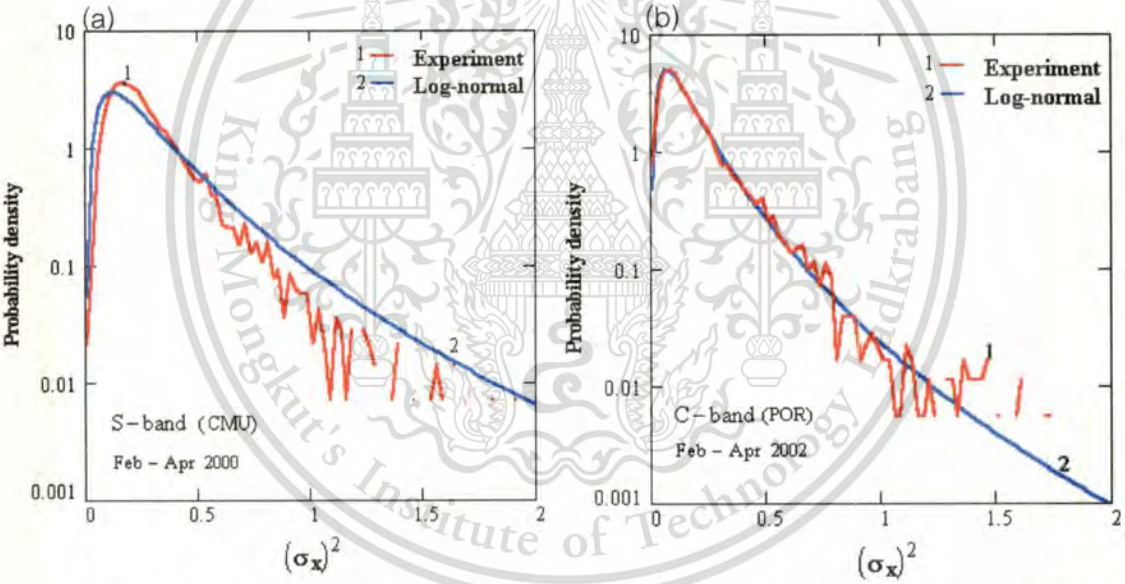

Figure 4.2 Distribution of variance. (a) S-band scintillation (b) C-band scintillation

From Figure 4.2 is the distribution function of variance given by log-normal distribution. Therefore, when the data of σ_x^2 take into natural log (log e), the experimental result become normal distribution, as shown in Figure 4.3a and 4.3c. The distribution function of variance will be accounted for long-term in the next section.

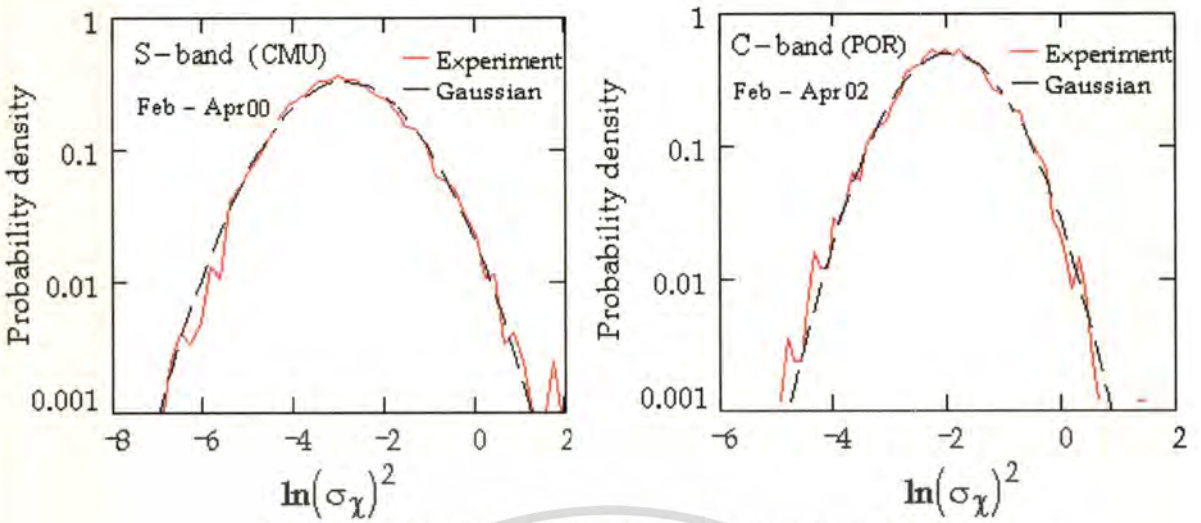

Figure 4.3 Probability density of log-amplitude scintillation

4.2 Long-Term Probability Density of Amplitude Scintillation

Amplitude scintillation results from the propagation of radio waves through the irregularities medium. The phenomenon of amplitude scintillation can be modeled through a random variable χ (unit in neper) such that at any points in time, the amplitude A of the received signal and the unfade amplitude A_0 are related to;

$$A(t) = A_0 \exp(\chi(t)) \tag{4.1}$$

where the probability density of amplitude fluctuation in decibels, $X(t)$

$$X(t) = 20(\log_{10} A - \log_{10} A_0) \text{ (dB)} = 8.686\chi(t) \tag{4.2}$$

4.2.1 Moulsley-Vilar Distribution

The Moulsley-Vilar model [13] for the long-term pdf of amplitude scintillation on slant path is based on Gaussian distribution in short-term and calculated the amplitude distribution function from the measured distribution of standard deviations. The process has a mean zero value the mathematical expectation of the probability density.

$$\langle p(\chi) \rangle = \int_0^\infty p(\sigma_\chi)\, p(\chi, \sigma_\chi)\, d\sigma_\chi \tag{4.3}$$

where $p(\chi, \sigma_\chi)$ is the Gaussian distribution function for given σ_χ, and χ is the deviation of amplitude scintillation from mean value. The amplitude scintillation is Gaussian distribution with a standard deviation σ_χ (known as the intensity of scintillation), given by

$$p(\chi,\sigma_\chi)=\frac{1}{\sigma_\chi\sqrt{2\pi}}\exp(-\frac{\chi^2}{2\sigma_\chi}) \tag{4.4}$$

and $p(\sigma_\chi)$ is the probability density function of the scintillation intensity σ_χ. However, it is useful to consider a process in which the variable σ_χ^2 is log-normal distribution. Therefore $\ln\sigma_\chi^2$ is Gaussian distribution:

$$p(\ln\sigma_\chi^2)=\frac{1}{\sigma_\sigma\sqrt{2\pi}}\exp\left(-\left(\frac{\ln\sigma_\chi^2-\ln\sigma_m^2}{2\sigma_\sigma^2}\right)^2\right) \tag{4.5}$$

where $\sigma_\sigma=\sigma(\ln\sigma_\chi^2)$ and σ_m^2 is median or mean of the distribution of scintillation intensity, $\overline{\ln\sigma_\chi^2}=\ln\sigma_m^2$. From the conventional transformation of probabilities [14], can be evaluate by

$$P_y(y)=\frac{P_x(x)}{|g'(x)|} \tag{4.6}$$

from $x=\ln\sigma_\chi^2$ and we assume $y=\sigma_\chi$ hence $x=\ln y^2$ and $y=\sqrt{\exp(\chi)}$ therefore;

$$g'(x)=\frac{dy}{dx}=\frac{\sqrt{\exp(x)}}{2}=\frac{\sigma_\chi}{2} \tag{4.7}$$

Substituting (4.5) and (4.7) in equation (4.6) is given as follows:

$$p(\sigma_\chi)=\frac{1}{\sigma_\sigma\sigma_\chi}\sqrt{\frac{2}{\pi}}\exp\left[-\frac{(\ln\sigma_\chi^2-\ln\sigma_m^2)^2}{2\sigma_\sigma^2}\right] \tag{4.8}$$

Combining equation (4.3), (4.4) and (4.8). Hence, the long-term probability density function of amplitude scintillations can be expressed as

$$p(\chi)=\frac{1}{\sigma_\sigma\pi}\int_0^\infty\frac{1}{\sigma_\chi^2}\exp\left[\frac{\chi^2}{2\sigma_\chi^2}-\frac{(\ln(\sigma_\chi^2/\sigma_m^2))^2}{2\sigma_\sigma^2}\right]d\sigma_\chi \tag{4.9}$$

4.2.2 Analytical approximation

All approximate form of the model for $p(\chi)$ presented in [1] has been obtained by usage of the Johnson-Su empirical distribution[15], which are a four-parameters distribution based on a transformation of a standard normal variate. Suppose y is the random variate, then the general expression for $p(y)$ is

$$p(y)=\frac{\eta}{\sqrt{2\pi}}\frac{1}{\sqrt{(y-\varepsilon)^2+\lambda^2}}\exp\left(-\frac{1}{2}\left(\gamma+\eta\ln\left[\left(\frac{y-\varepsilon}{\lambda}\right)+\sqrt{\left(\frac{y-\varepsilon}{\lambda}\right)^2+1}\right]\right)^2\right) \tag{4.10}$$

It can be done by using the method of moments, i.e., equating the first four moments of the test distribution $p(\chi)$ with those of the Johnson distribution and solving for the four parameters γ, η, ε and λ. However, the Moulsley-Vilar model has zero mean ($\varepsilon = 0$) and zero skewness ($\gamma = 0$). Therefore it can be shown that $p(y)$ reduces to a two-parameter, the approximate formulas for $p(\chi)$:

$$p(\chi) \approx \frac{\eta}{\sqrt{2\pi\left(\chi^2 + \lambda^2\right)}} \exp\left[-\frac{[F(\chi)]^2}{2}\right] \tag{4.11}$$

where $\chi = y - \varepsilon$, and $$\eta = \left[\frac{1}{2}\ln\left[\sqrt{6\exp\sigma_\sigma^2 - 2} - 1\right]\right]^{-1/2} \tag{4.12}$$

$$\lambda = \sigma_m \left(2\exp\left[\sigma_\sigma^2/2\right]\right)^{1/2} \left(\exp\left[2/\eta^2\right] - 1\right)^{-1/2} \tag{4.13}$$

Hence

$$F(\chi) = \eta \ln\left[\left(\frac{\chi}{\lambda}\right) + \left[\left(\frac{\chi}{\lambda}\right)^2 + 1\right]^{\frac{1}{2}}\right] \tag{4.14}$$

4.2.3 Experiment results of new model in Long-term

Designing the experimental results of new model in long-term has been developed by semi-empirical from new model in short-term and combining theoretical relations of Moulsley-Vilar distribution and experimentally observed dependencies. For long-term pdf of new model applied basic from Moulsley-Vilar distribution. That can be obtained by multiplying the pdf of the intensity and integrating over all values of σ_χ, from equation (4.3), can be rewritten as:

$$\langle nm(\chi) \rangle = \int_0^\infty nm(\sigma_\chi)\, nm(\chi, \sigma_\chi)\, d\sigma_\chi \tag{4.15}$$

That $nm(\chi, \sigma_\chi)$ is modified by new model in short-term and the experiment results in long-term as becomes to:

$$nm(\chi, \sigma_\chi) = \frac{1}{\sigma_\chi} \exp\left(\frac{-2.25}{5\sigma_\chi^2}\chi^2 - \frac{1}{10.5\sigma_\chi}\chi\right) \tag{4.16}$$

For equation (4.17) is applied from new model in short-term for use in long-term;

$$n(x) = \sigma_x \exp\left(\frac{-2.25}{5\sigma_x^2}(x-m)^2 - \frac{1}{10.5\sigma_x}(x-m) - \left(\sigma_x + \left(\frac{4.3 - 0.7\log\sigma_x^2}{5}\right)\left(\sqrt{\sigma_x^2} + \log\sigma_x^2\right)\right)\right) \tag{4.17}$$

and $nw(\sigma_\chi)$ can be obtained from equation (4.17) as following the process of Moulsley-Vilar and the conventional transformation of probabilities in equation (4.7). Therefor $nw(\sigma_\chi)$ is equal to:

$$nm(\sigma_\chi) = \frac{2\sigma_\sigma}{\sigma_\chi}\exp\left(\frac{-2.25}{5\sigma_\sigma}\left(\ln\left(\frac{\sigma_\chi^2}{\sigma_m^2}\right)\right)^2 - \frac{1}{10.5\sigma_\sigma}\left(\ln\left(\frac{\sigma_\chi^2}{\sigma_m^2}\right)\right) - d\right) \quad (4.18)$$

where $d = \sigma_\sigma + \left(\frac{4.3 - 0.7\log\sigma_\sigma^2}{5}\right)\cdot\left(\sqrt{\sigma_\sigma} + \log\sigma_\sigma^2\right)$ and $\ln\sigma_m^2$, σ_σ is similar to Moulsley-Vilar distribution. Therefore substitute (4.16) and (4.18) in (4.15), hence the experimental results of new model in long-term can be obtained:

$$\langle nm(\chi)\rangle = \int_0^\infty \frac{2\sigma_\sigma}{\sigma_x^2}\exp\left[\left(\frac{-2.25}{5\sigma_\sigma^2}\left(\ln\left(\frac{\sigma_x^2}{\sigma_m^2}\right)\right)^2 - \frac{1}{10.5\sigma_\sigma}\left(\ln\left(\frac{\sigma_\chi^2}{\sigma_m^2}\right)\right) - d\right) + \left(\frac{-2.25}{5\sigma_\chi^2}\chi^2 - \frac{\chi}{10.5\sigma_\chi}\right)\right] d\sigma_\chi \quad (4.19)$$

The experiment and model of the long-term pdf of amplitude scintillation $p(\chi)$ are shown in Figure 4.4, 4.5,4.6 and 4.7 at C-band, S-band and VHF respectively. That present the probability experiments in long-term compared with Gaussian, Moulsley-Vilar distribution, analytical approximation and experimental results of new model.

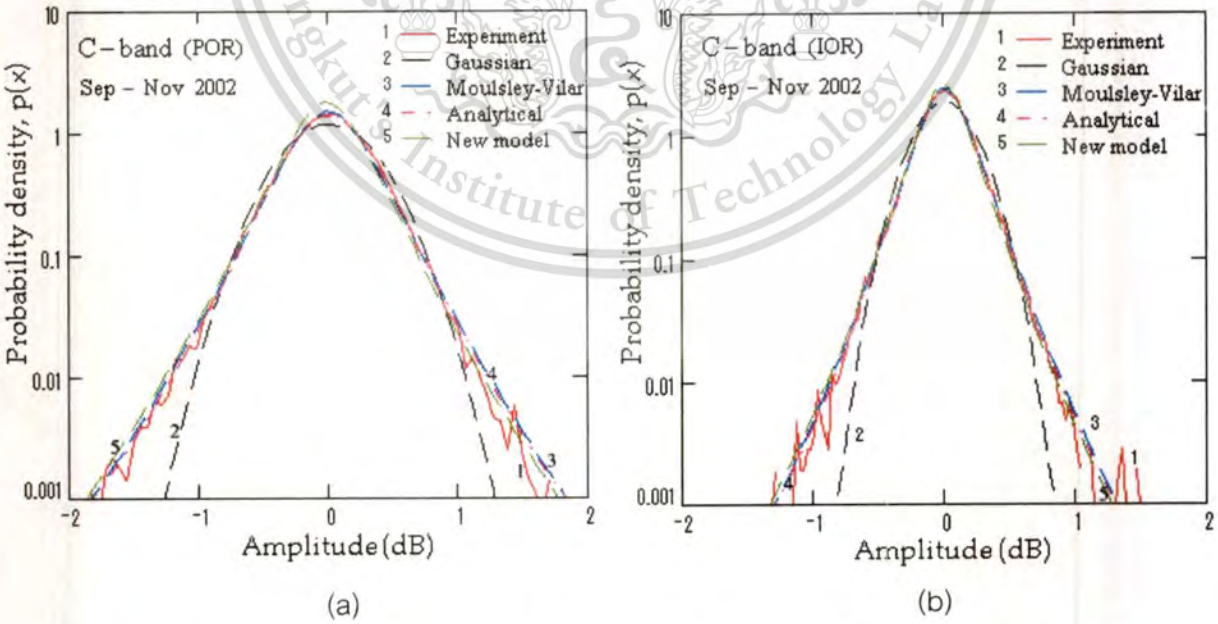

Figure 4.4 Comparison of probability of amplitude scintillation between each model (a) σ_m =0.288, σ_σ =0.81 and (b) σ_m = 0.181, σ_σ =0.881 in C-band scintillation

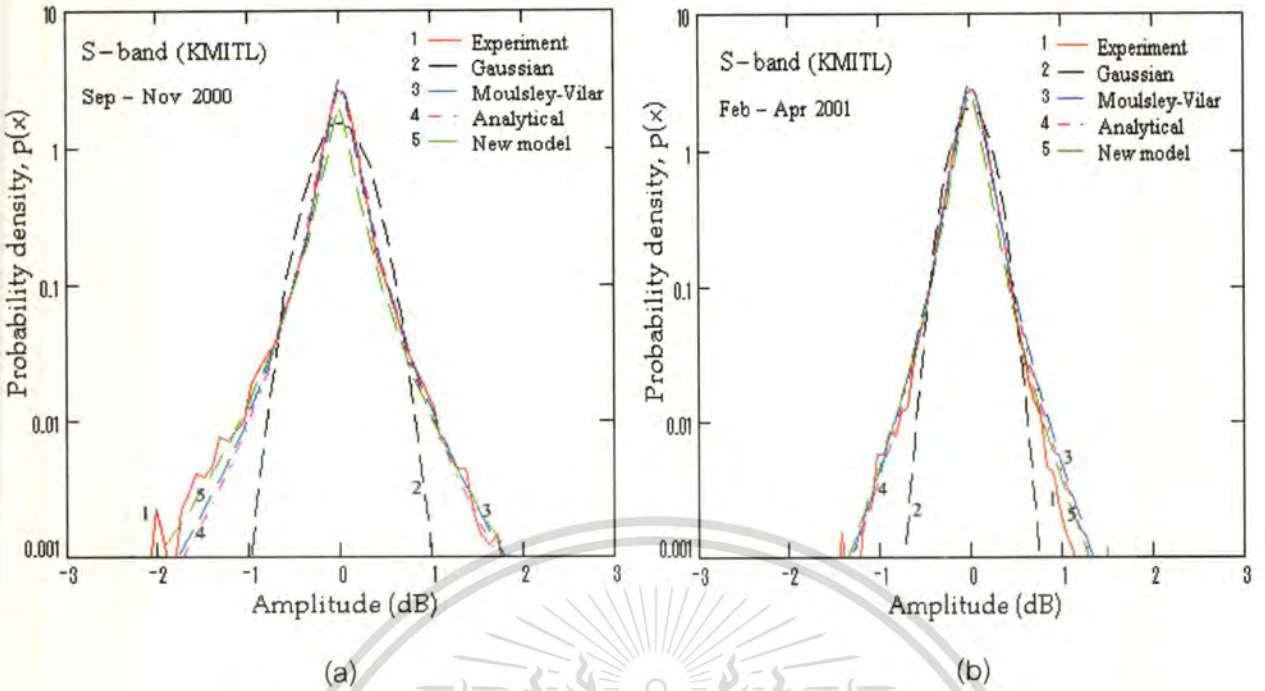

Figure 4.5 Comparison of probability of amplitude scintillation in S-band scintillation at KMITL (a) σ_m =0.147, σ_σ =1.409 and (b) σ_m = 0.141, σ_σ =1.125

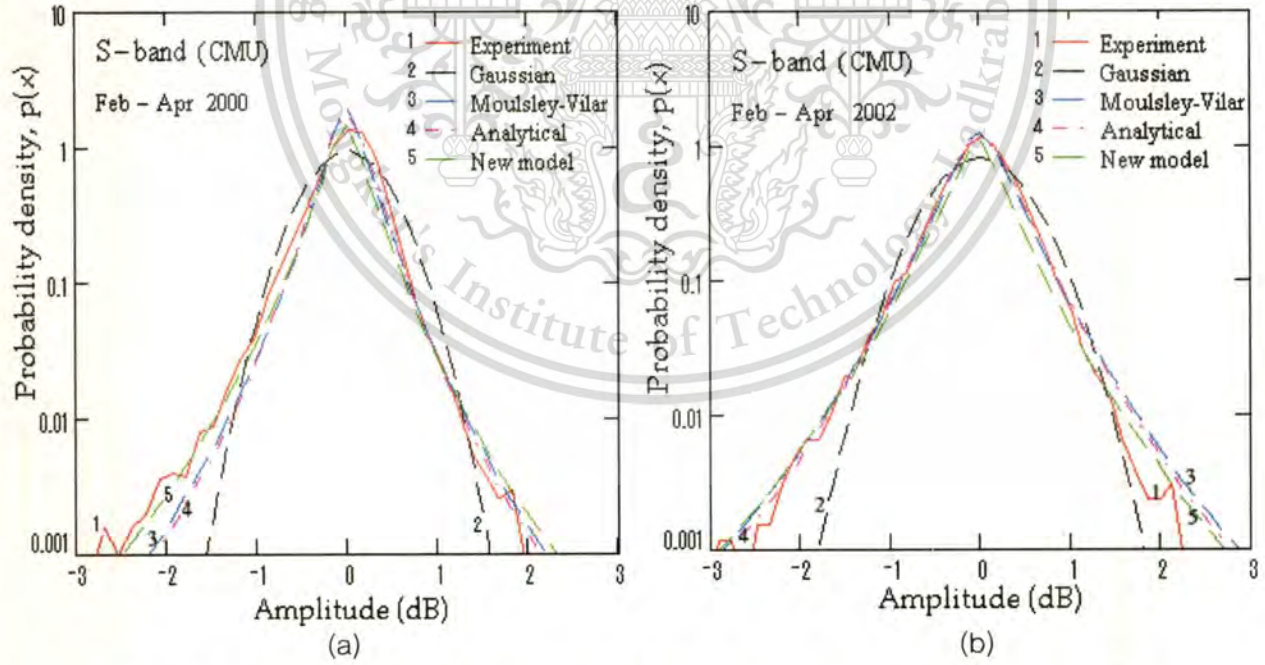

Figure 4.6 Comparison of probability of amplitude scintillation in S-band scintillation at CMU (a) σ_m =0.236, σ_σ =1.21 and (b) σ_m = 0.357, σ_σ =1.13

The probability density of the received amplitude was derived by the resulting distribution accounts for the seasonal variability (vernal equinox and autumnal equinox) of the scintillation intensity. These Figures present the amplitude scintillation in long-term from February-April and September-November. In Figure 4.5(a) and 4.6(a), the experimental results of new model (curve 5: green line) in the fade side are close to the Experiment (curve 1: red line) more than other models.

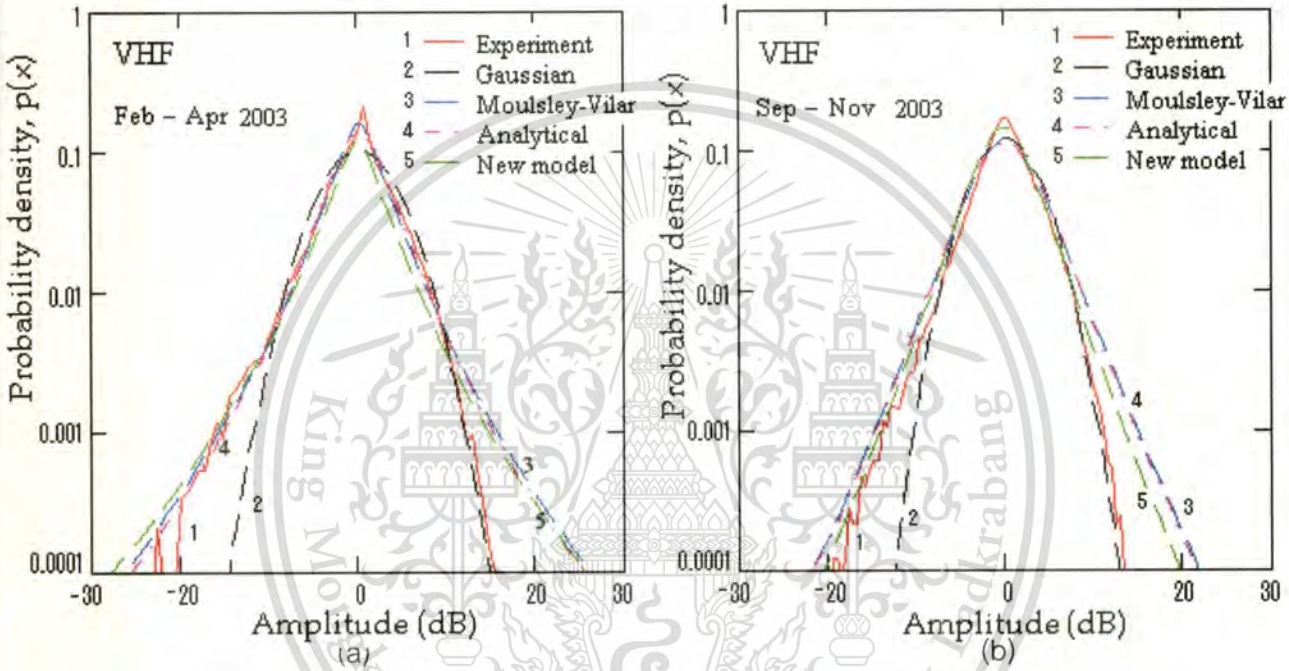

Figure 4.7 Comparison of probability of amplitude scintillation in VHF scintillation (a) σ_m =1.409, σ_σ =1.5523 and (b) σ_m = 0.92, σ_σ =1.802

In Figure 4.4–4.6 as curve 2 (black line) show the Gaussian distribution, it can be seen clearly that the curve 2 is not suitable to sampled data, especially in the tails. The results of Gaussian distribution obtain from the mean valued and standard deviation of the measured amplitudes. From Figure 4.7 in VHF, the amplitude scintillation in long-term can be seen that the experimental results is close to Gaussian distribution in the tail of enhancement side but for the tail of fade side appears closely to other model. For new model can be seen that the spread in the tail of experimental distribution is suitable more than Moulsley-Vilar distribution and analytical approximation. Although the analysis of statistic in experiment results of new model in long-term will consistent with

the experiment distribution but the data of amplitude scintillation is little data when considered in long-term especially in VHF and C-band. However, the amplitude scintillation in long-term can be evaluated by experiment results of new model in long-term, it will use this model in next section for estimation in the theoretical bit error rate.

4.3 Scintillation Fading on a Communication Link Performance

4.3.1 The SNR Parameter for Digital Communication Systems

The parameter E_b / N_o can be expressed as the ratio average signal power to average noise power, S/N (or SNR). Introducing the signal bandwidth W, we can write the identities showing the relationship between E_b / N_o and SNR for binary signals.

$$\frac{E_b}{N_o} = \frac{ST}{N_o} = \frac{S}{RN_o} = \frac{SW}{RN_oW} = \frac{S}{N}\left(\frac{W}{R}\right) \tag{4.20}$$

where S = average modulating signal power

T = bit time duration

$R = 1/T$ = bit rate

$N = N_oW$

Figure 4.8 illustrates the shape of most probability of error curves in the field of digital communications. The curve describes a system's error probability performance in terms of available E_b / N_o. For $E_b / N_o \geq x_o, P_E \leq P_o$. The dimensionless ratio E_b / N_o is a standard quality measure for digital communication system performance. It is noted that optimum digital signal detection implies a corrector (or matched filter) implementation, in this case, the signal bandwidth is equal to the noise bandwidth. We are often faced with a system model for which this is not the case; in practice, we include a factor in the required E_b / N_o that accounts for such suboptimal detection performance. Required E_b / N_o can be considered a metric which characterizes the performance of one system versus another; the smaller the required E_b / N_o, the more efficiency is the system modulation and detection process for a given probability of error [16].

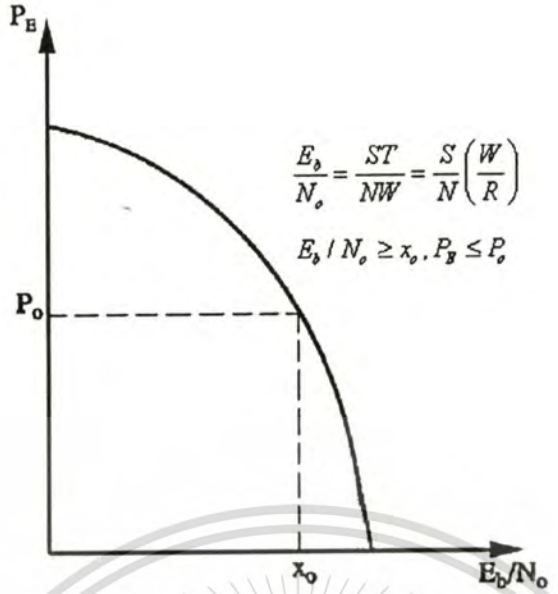

Figure 4.8 General shape of the P_E versus E_b / N_o curve.

In telecommunication transmission, the bit error rate (BER) is the percentage of bits that have errors relative to the total number of bits received in a transmission, usually expressed as ten to a negative power. The BER is an indication of how often a packet or other data unit has to be retransmitted because of an error. Too high a BER may indicate that a slower data rate would actually improve overall transmission time for a given amount of transmitted data since the BER may be reduced, lowering the number of packets that had to be re-sent.

4.3.2 Theoretical Bit Error Rate During Scintillation Fading

The ionospheric scintillation phenomenon is one of the most deleterious factors in communication system using the earth-space path. Every events cause performance degradation to these links when the signal fades below the specified margin i.e. below the gain allocated in the power budget of the system to overcome the effect. Not only the links using analog modulation techniques are effected but also the digitally modulated signals experience a disruption in communication as a drop in signal below the threshold of the modem increase the bit error rate. The increased bit error rate leads to either full or partial loss of a message, depending on the level of degradation.

Having shown the experiment results of new model in long-term, in either a parametric or the analytical from section 4.2, it is good enough for practical purposes, then it is possible to predict the average bit-error probability of a digital satellite link due to amplitude scintillations. The simplicity only binary transmission will be considered here. Then performs a transformation of probability to obtain the probability density of the signal-to-noise ratio, γ given as usual by

$$\gamma = \frac{A^2}{2N} \tag{4.21}$$

where N is the noise power in the receiver bandwidth and N is assumed to be constant and variations in γ are taken due to the variations in A cause by scintillation process, thus for unfade amplitude scintillation $\gamma_0 = A_0^2 / 2N$. From equation (4.1) can be represented as:

$$\chi = 10\log\left(\frac{\gamma}{\gamma_0}\right) \tag{4.22}$$

hence

$$\gamma = \gamma_0 10^{\frac{\chi}{10}} \tag{4.23}$$

For theoretical optimum detection of the binary signal, γ is equal to the energy (per bit) / noise ratio, (E_b/N_0). Over the whole fading process the average probability of bit error and the average E_b/N_0 are thus given by the expectations $\langle P_b \rangle$ and $\langle \gamma \rangle$.

$$\langle P_b \rangle = \int_{-\infty}^{\infty} P_b(Z(u))I(u)du \tag{4.24}$$

and

$$\langle \gamma \rangle = \int_{-\infty}^{\infty} Z(u)I(u)du \tag{4.25}$$

where $Z(u) = \gamma = \gamma_0 10^{\frac{\chi}{10}}$ and $I(u) = p(\chi)$, therefor

$$\langle P_b \rangle = \int_{-\infty}^{\infty} P_b(\gamma_0 10^{\frac{\chi}{10}})p(\chi)du \tag{4.26}$$

Two types of modulation formats will be considered in this section, they will illustrate the principles as following the probability of bit error for binary noncoherent frequency-shift-keying (NCFSK) and binary coherent phase shift keying (CPSK), therefore the perfect carrier acquisition is given by

NCFSK: $$P_b(\gamma) = \frac{1}{2}\exp(-\frac{\gamma}{2}) \quad (4.27)$$

CPSK: $$P_b(\gamma) = \frac{1}{2}erfc(\sqrt{\gamma}) \quad (4.28)$$

The theoretical probability of bit error is due to additive white Gaussian noise as a function of E_b/N_0 , γ for NCFSK and CPSK modulation are [17]

$$\langle P_b \rangle_{\text{NCFSK}} = \frac{1}{2}\int_{-\infty}^{\infty} \exp(-\frac{\gamma_0 10^{\frac{\chi}{10}}}{2})p(\chi)d\chi \quad (4.29)$$

$$\langle P_b \rangle_{\text{CPSK}} = \frac{1}{2}\int_{-\infty}^{\infty} (erfc(\sqrt{\gamma_0}10^{\frac{\chi}{20}}))p(\chi)d\chi \quad (4.30)$$

Thus the calculated $\langle P_b \rangle$ in equation (4.29) and (4.30) plotted against the average signal to noise ratio, $\langle \gamma \rangle$ in equation (4.31), is equation to:

$$\langle E_b/N_0 \rangle = \langle \gamma \rangle = \gamma_0 \int_{-\infty}^{\infty} 10^{\frac{\chi}{10}} p(\chi)d\chi \quad (4.31)$$

In Figure 4.9,4.11 and 4.13 indicate the theoretical $\langle P_b \rangle$ of CPSK and NCFSK plotted versus $\langle \gamma \rangle$ under condition of constant scintillation (σ_σ is constant) used Moulsley-Vilar distribution and experimental results of new model in long-term represent the $p(\chi)$. The Moulsley-Vilar distribution and experimental results of new model in long-term are dash and solid line respectively. As it can be seen from these Figures, when σ_m is increase, the efficient of performance will be decrease. The effect on $\langle P_b \rangle$ of the variability of σ_σ is shown in Figure 4.10, 4.12 and 4.14. Curves a, b and c as showing the effect of the variability of σ_x by keeping σ_m constant, and σ_σ increasing. For curves d) and e) are presenting the validity of the parameter in experimental results of $p(\chi)$. From these Figures, there are small differences between Moulsley-Vilar distribution and experimental results of new model. However, when consider the performance in case σ_σ is varied and can be seen from these Figure the experimental results of new model is little better.

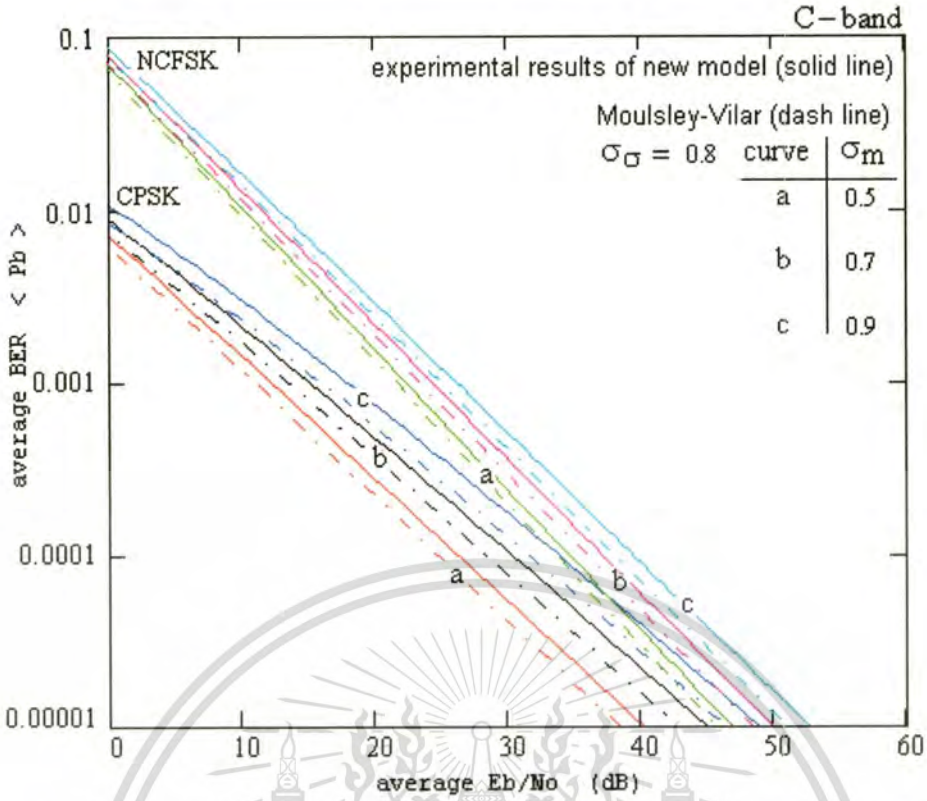

Figure 4.9 Average NCFSK and CPSK bit error rate for variable scintillation intensity in C-band

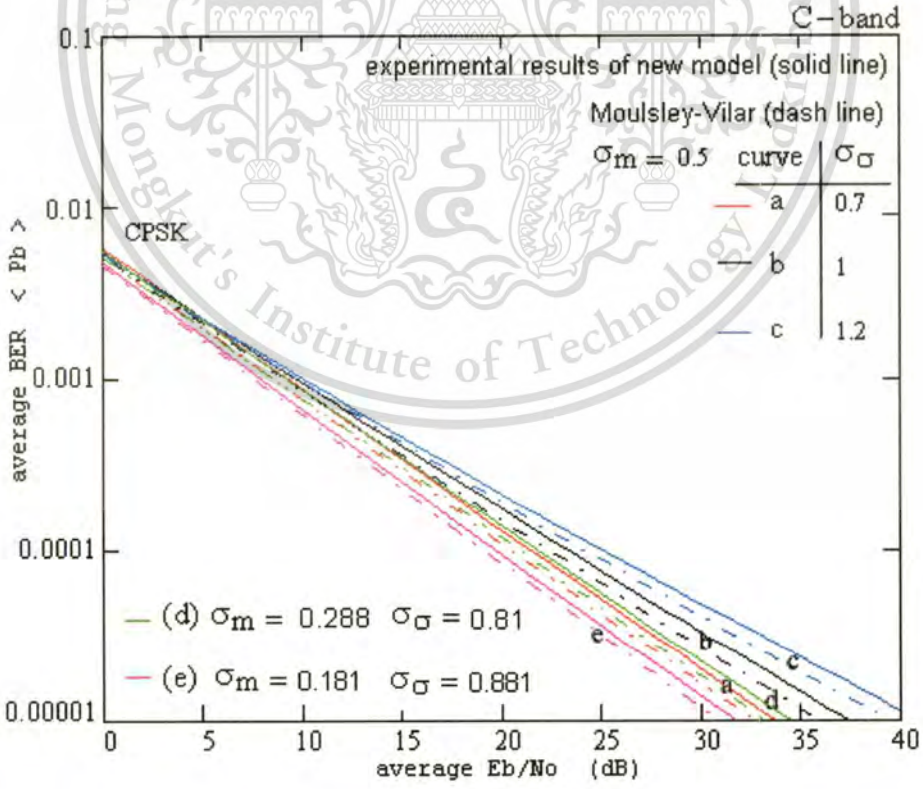

Figure 4.10 Average CPSK bit error rate for variable σ_σ and experiment parameter (d) σ_m =0.288, σ_σ =0.81 and (e) σ_m = 0.181, σ_σ =0.881 in C-band

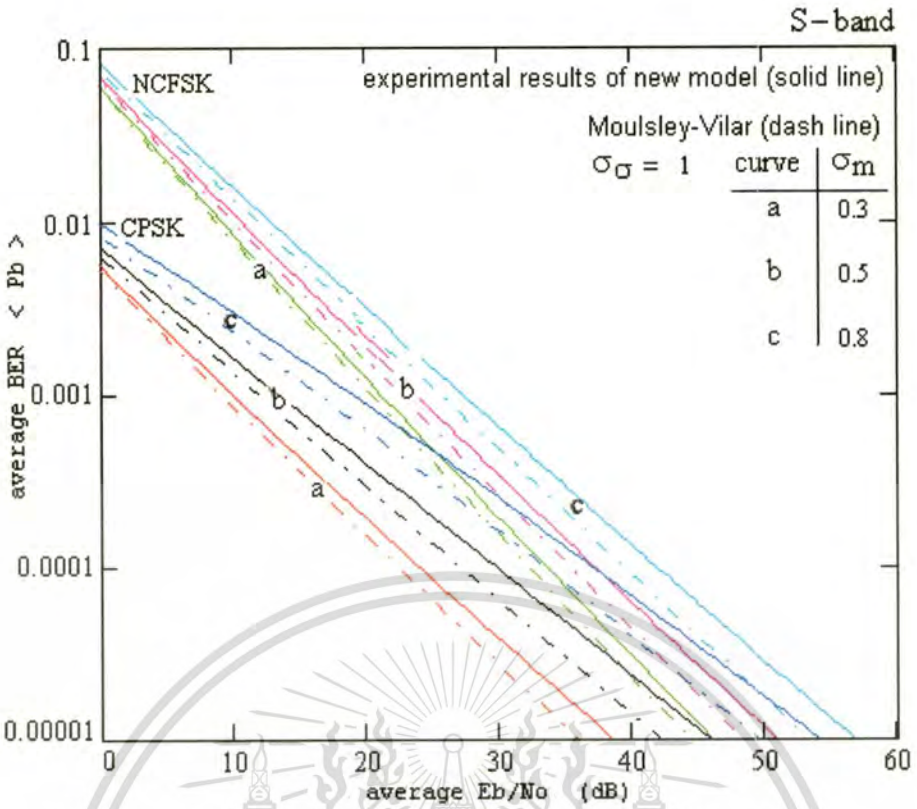

Figure 4.11 Average NCFSK and CPSK bit error rate for variable scintillation intensity in S-band

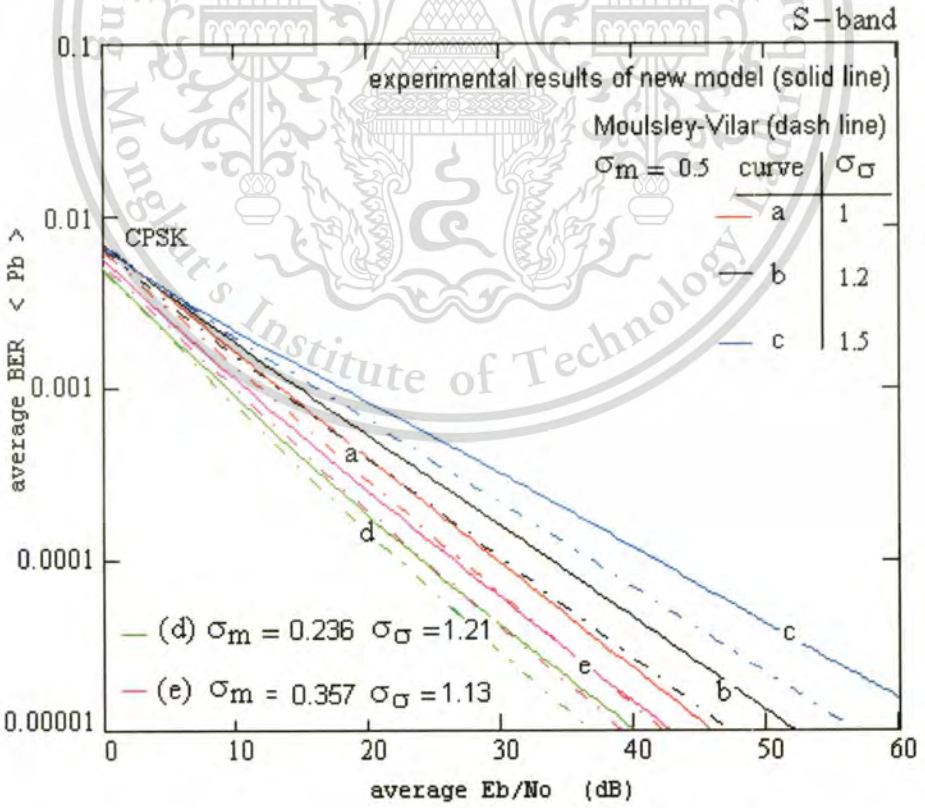

Figure 4.12 Average CPSK bit error rate for variable σ_σ and experiment parameter (d) σ_m =0.236, σ_σ =1.21 and (e) σ_m = 0.357, σ_σ =1.13 in S-band

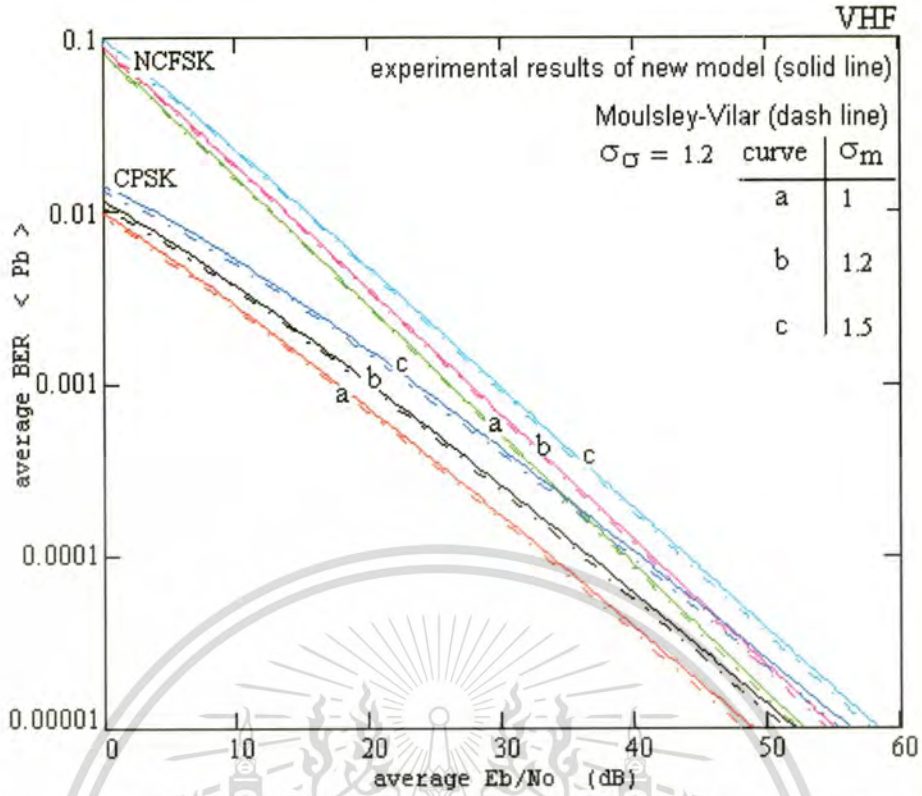

Figure 4.13 Average NCFSK and CPSK bit error rate for variable scintillation intensity in VHF

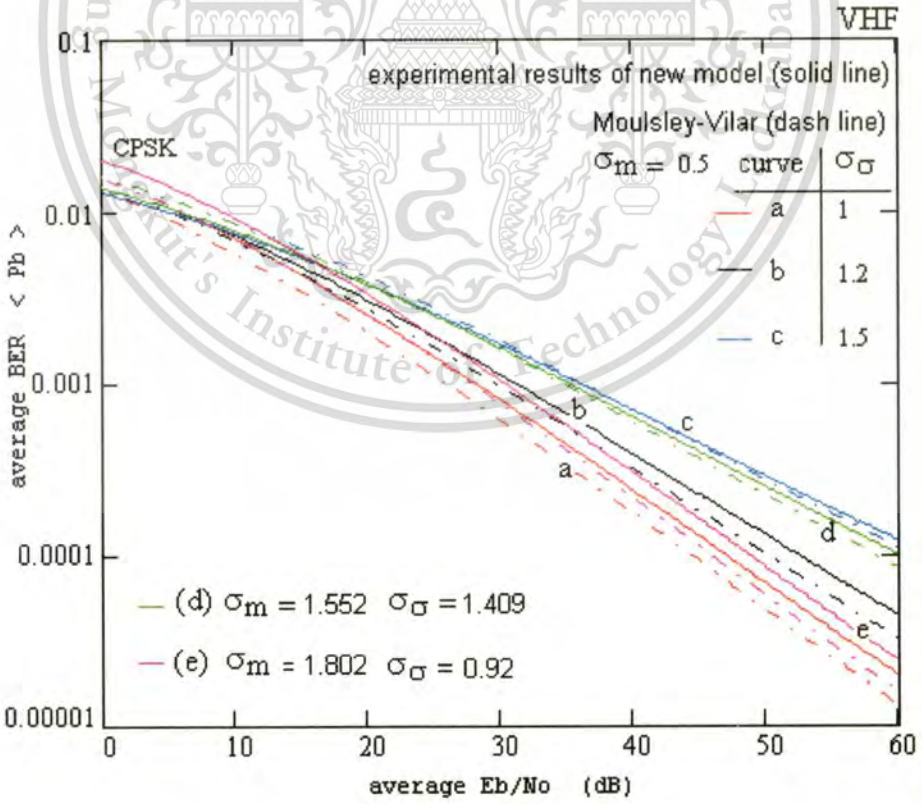

Figure 4.14 Average CPSK bit error rate for variable σ_σ and experiment parameter (d) σ_m =1.409, σ_σ =1.5523 and (e) σ_m = 0.92, σ_σ =1.802 in VHF

From Figure 4.9-4.14, when σ_m or σ_σ is higher, the average E_b/N_o required will be also increasing. The performance degradation can be expressed in term of the increase in average E_b/N_o required to bring the $\langle P_b \rangle$ under fading conditions to the same value as for the unfaded situation. Table 4.1-4.6 show example of the degradation at 10^{-4} from Figure 4.9-4.14 respectively. The E_b/N_o degradation at BER=10^{-4} present only experimental result of new model because there are small differences between these models.

Table 4.1 E_b/N_o degradation for various scintillation conditions in C-band by CPSK and NCFSK modulation

Condition, σ_σ =0.8		E_b/N_o degradation
Modulation Technique	σ_m	at BER=10^{-4} (dB)
CPSK	0.5	26.5
	0.7	30.1
	0.9	34.5
NCFSK	0.5	35
	0.7	36.8
	0.9	39.9

Table 4.2 E_b/N_o degradation for various scintillation conditions in C-band by CPSK modulation and using parameter in experiment

Condition,			E_b/N_o degradation
Modulation Technique	σ_σ	σ_m	at BER=10^{-4} (dB)
CPSK	0.7	0.3	21.25
	1	0.3	23.75
	1.2	0.3	25.1
Using parameter in experiment result of New model	0.81	0.288	21.5
	0.881	0.181	19.8

Table 4.3 E_b / N_o degradation for various scintillation conditions in S-band by CPSK and NCFSK modulation

Condition, σ_σ=1		E_b / N_o degradation at BER=10^{-4} (dB)
Modulation Technique	σ_m	
CPSK	0.3	24
	0.5	30
	0.8	36.2
NCFSK	0.3	33.5
	0.5	36.2
	0.8	41.8

Table 4.4 E_b / N_o degradation for various scintillation conditions in S-band by CPSK modulation and using parameter in experiment.

Condition,			E_b / N_o degradation at BER=10^{-4} (dB)
Modulation Technique	σ_σ	σ_m	
CPSK	1	0.5	29.8
	1.2	0.5	34
	1.5	0.5	42
Using parameter in experiment result of New model	1.21	0.236	24
	1.13	0.357	26.1

For Table 4.1, 4.3 and 4.5 as showing the average BER of CPSK and NCFSK modulation in case σ_m varied and they are obtained from Figure 4.9, 4.11 and 4.13. Table 4.2, 4.4 and 4.6, are indicated the average BER for variable scintillation intensity (σ_σ is varied) and parameter from experimental results for various conditions that corresponding to model in Figure 4.10, 4.12 and 4.14. This section has shown the significant degradation of BER performance can be expected during moderation to strong scintillations. Nevertheless, the values obtained for $\langle P_b \rangle$ are indicative of the amount of BER degradation to be expected.

Table 4.5 E_b / N_o degradation for various scintillation conditions in VHF by CPSK and NCFSK modulation

Condition, σ_σ =0.8		E_b / N_o degradation at BER=10^{-4} (dB)
Modulation Technique	σ_m	
CPSK	1	34
	1.2	37
	1.5	41
NCFSK	1	39.7
	1.2	42
	1.5	44

Table 4.6 E_b / N_o degradation for various scintillation conditions in VHF by CPSK modulation and using parameter in experiment

Condition,			E_b / N_o degradation at BER=10^{-4} (dB)
Modulation Technique	σ_σ	σ_m	
CPSK	1	1.5	45
	1.2	1.5	51.5
	1.7	1.5	62
Using parameter in experiment result of New model	1.409	1.552	60
	0.92	1.802	47

4.4 Conclusion

The long-term of amplitude scintillation can be analyzed the model by using Moulsley-Vilar distribution, analytical approximation and experiment results of new model. However Moulsley-Vilar distribution and analytical approximation, in some events will underestimation in the tail of Experiment distribution. In addition, the curves between Moulsley-Vilar distribution and analytical approximation are similar. However, for long-term scintillation of VHF, it is found that these models are close to the only fade side while the enhancement side is close to Gaussian distribution. For experimental results of

new model in long-term clearly appears with the experiment distribution more than Moulsley-Vilar distribution and analytical approximation.

In this chapter is derived the average BER by using binary CPSK and NCFSK modulation. The degradation of average BER for various conditions, which are quite apparent that the performance becomes worse as the variability σ_σ and σ_m increases. The variability parameter of σ_σ for earth-space path has been suggested by experiment observation in the range 0.5 to 1.5 [18]. However, the experimental results of the signal amplitude distribution obtain on VHF, S-band and C-band lead to values of $\langle P_b \rangle$ against $\langle E_b / N_o \rangle$ which agree well with the results obtained using the theoretical Moulsley-Vilar distribution and new model.

CHAPTER 5
CONCLUSION

5.1 Summary of the Study

Statistical analysis of amplitude scintillation due to ionospheric scintillation has been analyzed in VHF, S-band and C-band. The models of amplitude scintillation in short-term are presented by Gaussian distribution and Nakagami-m distribution to compare with the new model. In general the Gaussian distribution is close to the large enhancement while Nakagami-m distribution is close to the large fade. According to the experimental results in short-term, the new model is more suitable than Gaussian and Nakagami-m distribution on all these frequencies, especially in the large enhancement can be observed that the new model is more suitable than Gaussian distribution including strong scintillation cases. For Nakagami-m distribution in the strong scintillation case; especially VHF observed, it is not close to the large fade (when S_4 index is more than 0.8). The percentage of the correlation coefficient between experiment and new model is higher than Gaussian distribution. The percentage of the correlation coefficient between experiment and new model in S-band, VHF and C-band is 63%, 56% and 40% respectively. Therefore, the new model in short-term is the most suitable for S-band scintillation. However, the data of amplitude scintillation in S-band is much more than other frequencies. For cumulative distribution function of amplitude scintillation can be obtained the different value from 5% Peak and 95% Fade. However all scintillation events calculation can obtain the average receiver dynamic ranges which is appropriate for the scintillation characteristics in the particular station.

The long-term scintillation is analyzed by Gaussian distribution, Moulsley-Vilar distribution and analytical approximation including the experimental results of new model. These models depend on the parameter σ_σ and σ_m except the Gaussian distribution is based on mean value and standard deviation. The Gaussian distribution is not good for the experimental data in the long-term on S-band and C-band scintillation. While VHF scintillation in the enhancement side appears closely to Gaussian distribution more than other models. In addition, the Moulsley-Vilar distribution

and analytical approximation are underestimated in the tail of strong scintillation (summer). The observation of amplitude scintillation in long-term is consistent with experimental results of new model more than Moulsley-Vilar distribution and analytical approximation. The experimental results can be observed remarkably eventhough there are little data of amplitude scintillation during analysis in long-term. The theoretical estimation of the average bit error rate for digital link is subjected to scintillation fading is presented by CPSK and NCFSK modulations. The degradation of average BER for various conditions obviously appears that the performance becomes worse as the variability σ_σ and σ_m increases.

5.2 Remark for the Future Research

The prediction models of the effects of ionospheric scintillation should be analyzed in each frequency because in each frequency has various parameter such as frequency related to intensity of scintillation. In addition, the long-term amplitude scintillation should have data more than 3-4 years, especially in the year of solar maximum for analysis accuracy.

REFERENCES

[1] Jules Aarons, "Global Morphology of Ionospheric Scintillation," Proceedings of the IEEE, vol. 70, no. 4, April 1982.

[2] Recommendations ITU-R PN. 1057. "Probability distributions relevant to radiowave propagation modeling." 1994, pp. 27-40.

[3] K. Davies, Ionospheric Radio. Peter Peregrinus Ltd. 1990, London, United Kingdom

[4] http://www.dxlc.com/solar/solcycle.html

[5] T. Maruyama, Science of Space Environment. Tadanori Ondoh and Katsushide Marubashi eds. 2001

[6] K. Chie Yen and Chao-Han Liu, "Radio Wave Scintillations in the Ionosphere," Proceedings of the IEEE, vol. 70, no. 4, April 1982.

[7] B. H. Briggs and I. A. Parkin, "On the variation of radio star and satellite scintillation with zenith angle," J. Atmos. Terr. Phys., vol. 25, pp. 339-365, 1963.

[8] Recommendation ITU-R. "Ionospheric Propagation Data and Prediction Methods Required for the Design of Satellite Services and Systems." 1997, P.531-4.

[9] C. Bantin and R. G. Lyons, "The evaluation of satellite link availability," IEEE Trans. Comm., vol. COM-26, pp. 847-853, June 1978.

[10] O.P. Banjo, and E. Vilar, "Measurement and modeling of amplitude scintillations on low-elevation earth space paths and impact on communication systems," IEEE Trans. Comm., vol. COM-34, no.8, pp. 774-780, August 1986.

[11] P.K. Banerjee, R.S. Dabas, and B.M. Reddy, "C and L band transionospheric scintillation experiment: Some results for applications to satellite radio system." Radio Science, vol. 27, no.6, pp.955-969, November-December 1992.

[12] J. S. Bendat and A. G. Piersol, Random Data: Analysis and Measurement Procedure. New York: Wiley, 1971.

[13] T.J. Moulsley and E. Vilar, "Experimental and theoretical statistics of microwave amplitude scintillations on satellite downlinks," IEEE Trans. Antennas Propagat., vol. AP-30, pp. 1099-1106, Nov, 1982.

[14] Athanasios Papoulls. Probability, Random Variables and Stochastic Processes. 3rd Ed. Singapore: McGraw-Hill, Inc. 1991.

[15] N.L.Johnson, "Systems of frequency curves generated by methods of translation," Biometrika, vol.36, pp.149-176, 1949.

[16] Bernard Sklar, Digital Communication Fundamentals and application. Englewood Cliffs, NJ : Prentice Hall, c1988

[17] J.G.Proakis, Digital Communications. NewYork:McGraw-Hill 1983, pp. 467-469.

[18] O. P. Banjo, E. Vilar, "Binary error probabilities on earth-space link subject to scintillation fading," Electronics letters, vol. 21, no. 7, March 1985.

APPENDICES

APPENDIX A

Analysis of new model in Short-term

In this appendix we briefly discussion some the part of analysis of new model by nonlinear regression and Baye's Theorem. The analysis of new model has following by three components:

1. Nonlinear Regression

In many problems two or more variables are inherently related, and it is necessary to explore the nature of this relationship between two or more variable. Nonlinear regression is an important and powerful tool for data analysis. A nonlinear regression model can be expressed as

$$y_i = f(x_i, \beta) + e_i, \qquad i = 1, 2, ..., n$$

where $f(x_i, \beta)$ is a nonlinear function of the parameter vector β.

1.1 Generalized nonlinear regression

Very often, data is known to be best fit by certain model function. For example, perhaps you know that an exponential function provided the best fit for your particular data. A density $f(x, \beta)$ belongs to the exponential family of density functions, $f(x, \beta)$ can be expressed in the form

$$f(x, \beta) = e^{\beta_0 + \beta_1 x + ... + \beta_n x^n}$$

The exponential family of density functions provides a unified approach to estimation of the parameters in generalized models.

1.2 Parameter Estimation

In practice, depending on the application, we assume that the form of the nonlinear regression function $\mu_Y(x_1, ..., x_k)$ is known but it contains unknown parameters $\beta_1, ..., \beta_p$. We discuss point estimation for the unknown parameters in a nonlinear regression function using the method of least squares.

1.3 Least Squares Estimates of $\beta_1,...,\beta_p$

A popular method for estimating the unknown parameters in a nonlinear regression function is the method of least squares. According to this method, the estimates of $\beta_1,...,\beta_p$ are obtained by minimizing the quantity $\sum_{i=1}^{n} e_i^2$, the sum of squares of errors of prediction, where e_i is given by

$$e_i = y_i - \mu_Y(x_{i,1},...,x_{i,k})$$

As usual, the least squares estimates of $\beta_1,...,\beta_p$ are denoted by $\hat{\beta}_1,...,\hat{\beta}_p$. The estimated value of the subpopulation mean $\mu_Y(x_1,...,x_k)$ is denoted by $\hat{\mu}_Y(x_1,...,x_k)$. It is referred to as the fitted value corresponding to $x_1,...,x_k$ and is obtained by substituting the least square estimates of the parameters into the regression function. This is algebraically expressed by the equation

$$\hat{\mu}_Y(x_1,...,x_k) = \mu_Y(x_1,...,x_k;\hat{\beta}_1,...,\hat{\beta}_p)$$

The quantity $\hat{e}_i$ defined by

$$\hat{e}_i = y_i - \hat{\mu}_Y(x_{i,1},...,x_{i,k})$$

is called the residual corresponding to sample item i.

The minimum value for the sum of squares of errors of prediction corresponding to the least squares estimates $\hat{\beta}_1,...,\hat{\beta}_p$ is denoted by SSE, an abbreviation for the more complete notation $SSE(x_1,...,x_k)$. Thus

$$SSE = \sum_{i=1}^{n} \hat{e}_i^2 = \sum_{i=1}^{n} \left[y_i - \hat{\mu}_Y(x_{i,1},...,x_{i,k}) \right]^2$$

and, as in linear regression, we refer to SSE as the sum of squared errors.

1.4 Computation of Least Squares Estimates

In the case of multiple linear regression, the least squares estimates of the parameters $\beta_1,...,\beta_p$ can be computed quite easily using formula. However, the estimation of parameters in nonlinear regression models usually requires the use of iterative methods on digital computers, and explicit formulas for the estimates are generally not available.

2. Probability Distribution

Then a probability distribution or probability density function (pdf) of X is a function $f(x)$ such that for any two numbers a and b with $a \le b$,

$$P(a \le X \le b) = \int_a^b f(x)dx$$

That is, the probability that X takes on a value in the interval $[a,b]$ is the area above this interval and under the graph of the density function. The graph of $f(x)$ is often referred to as the density curve.

For $f(x)$ to be a legitimate pdf, it must satisfy the following two conditions:

1. $f(x) \ge 0$ for all x
2. $\int_{-\infty}^{\infty} f(x)dx$ = area under the entire graph of $f(x) = 1$

For design model is probability distribution. The analysis of new model is applied by Bayes' theorem.

3. Bayes' Theorem

The law of total probability can also be used to derive an important formula called Beayes' Formula. Bayes' theorem can be expressed in discrete form, as follows:

$$P(s_i / z) = \frac{P(z / s_i)P(s_i)}{P(z)} \quad \text{and} \quad i = 1,...,M$$

where $$P(z) = \sum_{i=1}^{M} P(z / s_i)P(s_i)$$

Therefor, this thesis is applied these method for new model. That equation is showing in equation (3.6) and (3.8)

APPENDIX B

The correlation coefficient

Correlation is a statistical technique which can show whether and how strongly pairs of variables are related. That the correlation is a single number that describes the degree of relationship between two variables. The sample correlation coefficient recall that the correlation:

$$Corr(X,Y) = \frac{Cov(X,Y)}{\sqrt{Var(X)Var(Y)}}$$

The sample correlation coefficient, r (also know as the Pearson product moment correlation coefficient) for a set of paired data observations (x_i, y_i) is

$$r = \frac{S_{XY}}{\sqrt{S_{XX}}\sqrt{S_{YY}}} = \frac{\sum_{i=1}^{n}(x_i - \bar{x})(y_i - \bar{y})}{\sqrt{\sum_{i=1}^{n} x_i^2 - n\bar{x}^2}\sqrt{\sum_{i=1}^{n} y_i^2 - n\bar{y}^2}}$$

$$= \frac{\sum_{i=1}^{n} x_i y_i - n\bar{x}\bar{y}}{\sqrt{\sum_{i=1}^{n} x_i^2 - n\bar{x}}\sqrt{\sum_{i=1}^{n} y_i^2 - n\bar{y}^2}}$$

Propertied of r : the most important properties of r are as follows.

1. The value of r does not depend on which of the two variables under study is labelled x and which is labelled y
2. The value of r is independent of the units in which x and y are measured.
3. The value of r may take on any value between plus and minus one. $(-1 \le r \le 1)$

AUTHOR BIOGRAPHY

Author: Miss Viparat Torchakul

Date of Birth: October 9, 1978

Bachelor Degree: B.Eng. Electronic Engineering

Institute: Department of Electronic Engineering

Faculty of Engineering

The University of the Thai Chamber of Commerce (UTCC)

Year of Graduation: 2000

Interested researches: Ionospheric Scintillation, Radio wave propagation

Related Publication:

1. V. Torchakul, K. Visessiri, K. Makaratat, N. Leelaruji, N. Hemmakorn, "Modeling of Amplitude Scintillation and Intensity in different geomagnetic latitude on S-band (1.694 GHz)," *Proceeding The Third International Symposium on communications and Information Technologies,* Songkhla, Thailand, vol. 1, Sep 2003, pp. 150-153.
2. V. Torchakul, K. Visessiri, P. Theerapatpaiboon, N. Leelaruji, N. Hemmakorn, "Experimental of modeling scintillation distribution in short-term on S-band (1.694 GHz)," *Proceedings of The First Electrical Engineering/Electrical, Computer, Telecommunications, and Information Technology (ECTI) Annual Conference,* Pattaya, Cholburi, Thailand, May 2004, pp.429-432.